American Journal of Remote Sensing
2025, Vol. 13, No. 2, pp. 48-72
https://doi.org/10.11648/j.ajrs.20251302.11

Research Article

Field-Scale Monitoring of Rice Crop Using Open-Source Satellite Data and Digital Platforms - A Case Study of Samastipur District, Bihar, India

Srikanth Rupavatharam[1,*], Pranuthi Gogumalla[1], Jameeruddin Shaik[1], Suman Saraswathibatla[2], Mukund Patil[1]

[1]Digital Agriculture, International Crops Research Institute for the Semi-Arid Tropics, Hyderabad, India
[2]Dr. Reddy’s Foundation, Hyderabad, India

Abstract

Crop monitoring over large areas with high accuracy is of great significance in precision agriculture. The study is an attempt to assess the potential of open-source high-resolution satellite datasets and open-source digital platforms in combination with AI/ML algorithms for near-real-time crop monitoring and yield estimation at the farm level. In this research, we used Sentinel-1 and Sentinel-2 datasets, by processing them on the Google Earth Engine platform and developed several crop-based indicators to assess crop phenology as well as the distinction between a well-managed field (demo plots) vs a normal farmers' practice-managed crop (control plots) using Sentinel-1 satellite data. Further, crop yields were estimated before the harvesting of the crop by using Sentinel-1 and Sentinel-2 data with machine learning algorithms. The findings demonstrate that the effect of an improved package of practices on rice was significantly different from the farmer's practice. Among the statistical yield models developed for yield estimation, the gradient tree boosting model performed better than other models. This study proposes a novel method of near-real-time remote crop monitoring right from sowing to harvest time to estimate crop yields with an accuracy of 77 percent. There is potential in using open-source satellite data for monitoring farm fields in the future.

Keywords

Precision Agriculture, Crop Yield Estimation, Sentinel 1 & 2 Satellite Data, Google Earth Engine, Machine Learning, Remote Sensing

1. Introduction

Rice is the staple food for a large proportion of India’s population, and its reliable production plays a vital role in ensuring national food security. Bihar is one of the major rice-producing states, where districts like Samastipur contribute significantly to both household consumption and market supply. However, rice cultivation in the region is highly sensitive to climatic variability, water availability, and biotic stresses, which pose challenges for accurate yield forecasting and effective agricultural planning. Traditional agricultural monitoring methods, such as field surveys and agronomic models, provide valuable insights into crop conditions and yield estimates [1]. However, these approaches are

*Corresponding author: Srikanth.Rupavatharam@icrisat.org (Srikanth Rupavatharam)

Received: 8 September 2025; **Accepted:** 23 September 2025; **Published:** 30 October 2025

labor-intensive, time-consuming, and limited in spatial coverage. Recent advancements in remote-sensing technologies have transformed agricultural monitoring by providing timely, spatially extensive, and multidimensional datasets. Over the past decade, there has been a rapid increase in the use of satellite-based remote sensing for crop monitoring and vegetation mapping. These include optical products (e.g., MODIS, Landsat, Sentinel-2, and SPOT), Synthetic Aperture Radar (SAR), and microwave sensors (e.g., RADARSAT, ALOS PALSAR, and Sentinel-1) [2-4].

Optical remote sensing, particularly Sentinel-2, offers high-resolution imagery for detailed assessment of crop types, health, and vegetation indices [5, 6]. However, optical sensors are weather-dependent and often constrained during the Kharif (monsoon) season due to persistent cloud cover. In contrast, SAR-based systems, such as Sentinel-1, provide robust imaging capabilities unaffected by clouds or illumination conditions, making them highly effective for monitoring rice during monsoon [7, 8]. The integration of Sentinel-1 SAR data with Sentinel-2 optical data presents a significant advancement in crop monitoring and yield prediction [9-11]. By leveraging these complementary datasets, agricultural monitoring systems can more accurately detect and quantify crop conditions at higher temporal frequencies, thereby improving the robustness of yield predictions and supporting informed decision-making for food security [12-14].

In parallel, machine learning (ML) techniques such as Random Forest (RF) and Artificial Neural Networks (ANN) have been increasingly employed in agriculture to enhance predictive modeling and decision-making [15-17]. These methods can capture complex nonlinear relationships between crop growth parameters and remote-sensing indices. The use of ML algorithms, combined with open-source satellite data, enables near-real-time monitoring of crop health and yield at minimal cost, even in remote locations.

Accurate regional crop monitoring requires precise spatiotemporal phenological data. SAR systems have proven particularly useful for monitoring rice crop across phenological stages. Both X-band [18-20] and C-band [21, 22] sensors have shown promise, with radar backscatter coefficients emerging as reliable indicators of rice crop calendar variations. Several studies have demonstrated the potential of Sentinel-1 data to identify crop calendars [23-25]. For instance, Huijin et al. (2021) employed Sentinel-1 VH time series to track rice crop calendars [26], while Manago et al. (2020) estimated transplanting dates using Sentinel-1, a methodology that has been adapted in this study [27].

Although SAR has been widely used for rice mapping and monitoring, limited research has addressed the effects of crop management practices on growth and yield, owing to the challenges of observing these practices and their variability across fields. A few studies have examined the impact of variable planting using Sentinel-1 [28, 29]. Traditionally, crop yield prediction has been based on statistical and process-based models, which simulate the physical mechanisms of crop growth and yield formation [30, 31]. Remote sensing (RS) data have been increasingly integrated into these models to improve their applicability at regional scales [32]. However, process-based models are often resource-intensive and require detailed local data, while conventional statistical models struggle to capture nonlinear interactions among variables [33]. Machine learning approaches, including Support Vector Machines (SVM), Decision Trees (DT), and Random Forests (RF), have recently shown strong potential for agricultural mapping and yield estimation [34-38]. By leveraging remote sensing and ML, this study aims to bridge the gap between large-scale monitoring and actionable insights at the regional scale.

Although Sentinel-1 and Sentinel-2 have proven valuable for crop monitoring, their potential for continuous rice crop status assessment throughout the growing season remains underexplored. This study aims to establish robust relationships between rice growth parameters and remote sensing-derived indices to improve yield prediction.

The objectives of this study are to:

1) Monitor rice crop growth and development using satellite-derived indices.
2) Compare and analyze rice yields from control and demonstration plots using satellite-based estimates.
3) Develop yield prediction models using Sentinel-1 and Sentinel-2 indices as proxies for yield.
4) Develop a crop monitoring system (CMS) and an interactive web interface to host datasets and results.

2. Materials and Methods

2.1. Study Area

Samastipur district in Bihar lies in the Indo-Gangetic plains and is faced with severe flooding every *Kharif* leading to huge crop losses. The district is spread over an area of 2904 km^2 and agriculture is the district's main economic occupation, employing approximately 83 percent of the total working population (Figure 1). The district is noted for its fertile alluvial soil. Rice and Wheat are major crops in the district with an average net sown area of 184 thousand ha and a cropping intensity of 137 percent. Rice is the major *Kharif* crop with an average sown area of 69 thousand ha, and similarly, wheat is the major crop grown during Rabi with an average sown area of 59 thousand hectares under irrigated conditions.

2.2. Ground Truth Data

Ground truth data was collected for the *Kharif* seasons 2020-21 and 2021-22 on aspects like geographical coordinates of the demo and control plots, crop sown, date of sowing, crop variety sown, seed treatment, and fertilizer application. For the *Kharif* 2020-21 experiments were conducted in 542 demo and 542 control plots but due to heavy rains and flooding, only 42 demo and 40 control plots could be sampled. Similarly, for *Kharif* 2021-22, the study was conducted in 459 demo and 459 control plots but due to flooding, inconsistencies in the latitude and longitude values provided, duplicated data, and zero yield values, only 280 demo and 45 control plots were used in this study. Management practices recommended for rice crops in the Samastipur district were adopted in demo plots and adopted the traditional method of growing rice crops by farmers of Samastipur in control plots. The recommended package of practices for the rice crop is detailed in (Table 1). After several research trials by agricultural research organizations, scientists have proposed an improved package of practices to be adopted for higher yields in rice in the Samastipur district. However, farmers still cling to the old traditional methods, which give very low yields. In demo plots, both the traditional method of tillage and zero tillage practice have been adopted, while in control plots, farmers adopted only the traditional method of tillage. In this research, we tried to compare the demo and control plots and the impact of these management practices on the growth and yields of Rice crops using satellite data.

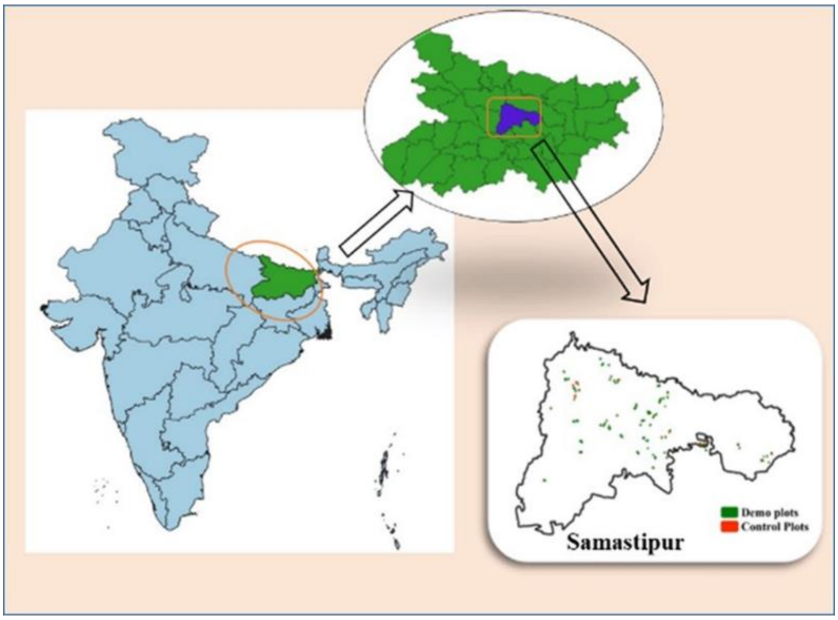

Figure 1. *Study area showing the location of demo (green colored points) and control (red colored points) plots in Samastipur district in Bihar, India. Maps were prepared using QGIS 3.42.0 (https://qgis.org/).*

2.3. Sentinel-1 & 2 Data

Sentinel-1 mission provides data from a dual-polarization C-band Synthetic Aperture Radar (SAR) instrument at 5.405GHz (C band). This collection includes Sentinel-1 Ground Range Detected (GRD) scenes, processed using the Sentinel-1 Toolbox to generate a calibrated, ortho-rectified product. Each scene was pre-processed with Sentinel-1 Toolbox using: 1) thermal noise removal, 2) radiometric calibration, and 3) terrain correction using SRTM 30 or ASTER DEM for areas greater than 60 degrees' latitude. The final terrain-corrected values are converted to decibels (dB) via log scaling (10*log10(x)). The data is provided at an outstanding time interval of 10 days and a spatial resolution of 10 m [39].

Sentinel-2 is a wide-swath, high-resolution, multispectral imaging mission with a global 5-day revisit frequency. The Sentinel-2 Multispectral Instrument (MSI) samples 13 spectral bands: visible (3 bands) and NIR (2 bands) at 10 meters, red edge (3 bands), and Short-wave infrared (SWIR) (2 bands) at 20 meters' spatial resolution, and atmospheric bands at 60-meter spatial resolution 15. It provides data suitable for assessing the state and change of vegetation, soil, and water cover. However, we have very limited cloud-free images for the *Kharif* seasons [40].

The availability of Sentinel-1 and Sentinel-2 data during the rice crop growth period for *Kharif* 2020-21 and *Kharif* 2021-22 is given in (Figure 2). Sentinel-1 data denoted using long blue lines shows that the data was available throughout the cropping period as it was not intercepted by clouds or the time of the day. So, for the study, we had 30 Sentinel-1 images during the *Kharif* 2020-21 and *Kharif* 2021-22 each with at least 4 images for each month. Sentinel-2 images available for *Kharif* 2020-21 and *Kharif* 2021-22 were 37, however, only 11 and 9 Sentinel-2 images for *Kharif* 2020-21 and *Kharif* 2021-22 could be used in the study which has cloud cover of < 20 percent (denoted using green long lines) while the remaining 26 and 28 images for *Kharif* 2020-21 and Kharif 2021-22 respectively had a cloud cover of more than 20 percent (orange lines) were not useful in this study. Bands and vegetation indices developed from Sentinel-1 and Sentinel-2 data are presented in (Table 2).

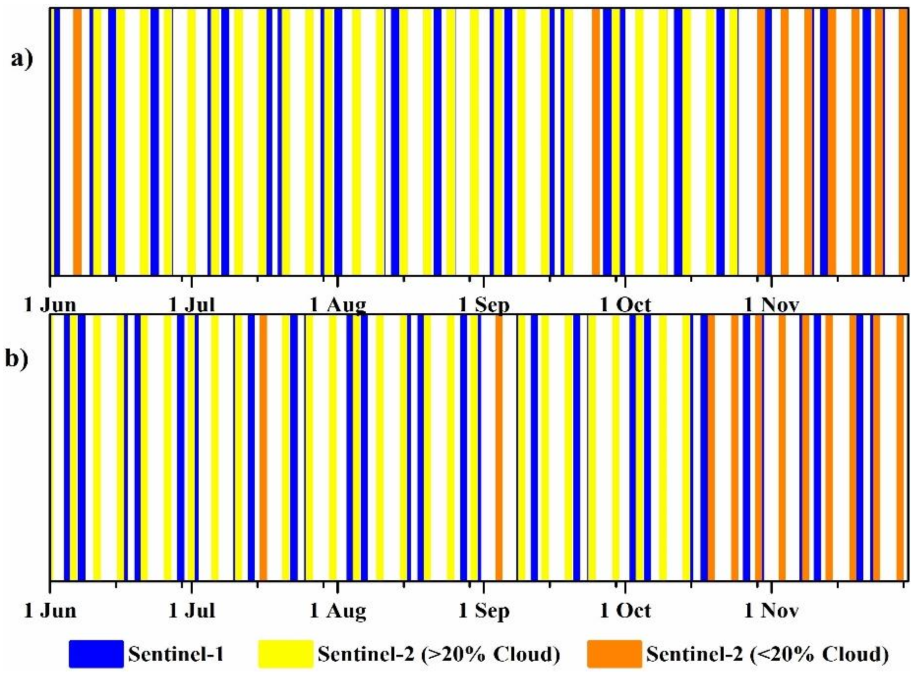

Figure 2. *Availability of Sentinel-1 and Sentinel-2 data during a) Kharif 2020-21 and b) Kharif 2021-22 (starting from 1st June to 30th November) for Samastipur district. Graphs were prepared using Origin Pro v 9.1 software (https: //www.originlab.com/origin).*

2.4. Google Earth Engine (GEE) & Preprocessing of Satellite Data

Google Earth Engine is a cloud computing platform that allows users to run geospatial analysis on Google's infrastructure. Google Earth Engine combines a multi-petabyte catalog of satellite imagery and geospatial datasets with planetary-scale analytical capability. Scientists, researchers, and developers use Earth Engine to detect changes, map trends, and quantify differences on the Earth's surface. GEE has a data repository that includes more than thirty years of historical imagery and scientific datasets, updated and expanded daily. It contains over forty petabytes of geospatial data instantly available for analysis. The Earth Engine Code Editor (code.earthengine.google.com) is a web-based IDE (Integrated Development Environment) for the Earth Engine JavaScript API (Applications Program Interface) [41].

The Sentinel-1 Ground Range Detected (GRD) ascending data and Sentinel-2 Harmonized dataset were pre-processed in GEE to generate analysis-ready inputs for crop monitoring and yield estimation. For Sentinel-1, preprocessing involved thermal noise removal, radiometric calibration to sigma nought backscatter coefficients (dB), and terrain correction using the SRTM 30 m DEM to correct geometric distortions and geocode the imagery [42]. Only VH and VV polarizations from the ascending pass were retained, with speckle filtering optionally applied to reduce noise. Sentinel-2 Harmonized surface reflectance data, which are atmospherically corrected via Sen2Cor, were further processed by applying cloud and shadow masking using the QA60 band and the s2cloudless algorithm, followed by scaling of reflectance values to surface reflectance using appropriate scale factors [43]. Spectral bands were then used to derive vegetation indices and cloud-free observations were composited over defined temporal intervals to create consistent time series inputs. Together, these preprocessing steps ensured that both radar and optical datasets were harmonized, cloud-free, and suitable for downstream modelling and yield estimation.

Table 1. *Management Practices adopted in Demo and Control Plots.*

S. No	Management Practices	Demo Plots	Control Plots
1	Seed treatment	Seed treated with 0.2-gram streptocyclin and 0.2-gram Carbendazim/Bavistin/ Mancozeb per kg of seed before sowing	Seed treatment adopted in 21 control plots
2	Nursery management	Seed rate - 35-40 kg ha^{-1}. Nutrient- 50-40-40 kg N-P$_2$O^5-K$_2$0 ha^{-1} +	Seed rate - not defined. Nu-

S. No	Management Practices	Demo Plots	Control Plots
		5 t FYM ha^{-1}	trient - Nil
3	Transplanting	Seedling age: 35-40 days 2-3 seedlings hill-1 at 15 cm x 15 cm or 15 cm x 20 cm spacing.	Seedling age - 21-25 days
4	Nutrient management	120-60-40 kg N*-P_2O_5-K_20 ha^{-1} + 5t FYM ha^{-1}	Farmer's practice

Table 2. Bands and Indices (vegetation and moisture based) developed from Sentinel-1 and Sentinel-2.

Satellite/Sensor	Index	Full form/region
Sentinel-1 (SAR)	VH	Vertical Horizontal Dual-Polarized band [39]
	VV	Vertical Vertical Dual Polarized band [39]
	VH/VV	Ratio of VH and VV [39]
	VV/VH	Ratio of VV and VH [39]
Sentinel-2	B2	Blue [40]
	B3	Green [40]
	B4	Red [40]
	B5	Red Edge1 [40]
	B6	Red Edge2 [40]
	B7	Red Edge3 [40]
	B8	NIR1 [40]
	B8A	NIR2 [40]
	B11	SWIR1 [40]
	B12	SWIR2 [40]
	NDVI	Normalized Differential Vegetation Index [44]
	RENDVI	Red-Edge Normalized Differential Vegetation Index [42]
	PRIN	Photochemical Reflectance Index [45]
	REIP	Red Edge Inflection Point [46]
	MSI1	Moisture Stress Index1 [42]
	MSI2	Moisture Stress Index2 [42]
	NMDI	Normalized Multiband Drought Monitoring Index [47]
	NMSI1	Normalized Moisture Stress Index1 [42]
	NMSI2	Normalized Moisture Stress Index2 [42]
	DWSI	Disease water stress index [48]

2.5. AI/ML Algorithms for Crop Monitoring

Artificial intelligence (AI) and machine learning (ML) models have become increasingly important in agriculture, offering innovative solutions to various challenges faced by farmers and stakeholders in the agricultural sector [49-51]. These models leverage advanced algorithms to analyze vast amounts of data, enabling better decision making, resource optimization, and increased productivity.

AI/ML uses remote sensing data analysis to monitor crop health, identify patterns, and classify crops [52, 53]. These models also predict crop yields, detect diseases and pests, manage weeds, and optimize nutrient management. They also assess water stress in crops, allowing farmers to adjust their irrigation schedules and conserve water resources. Harvest forecasting and management are based on real-time data, which helps farmers plan harvesting operations. AI/ML models also aid in climate change adaptation by providing insights into climate variability and extreme weather events. These tools help farmers make informed decisions about crop rotation, land-use patterns, and agricultural practices, ultimately improving crop productivity and resilience.

Linear regression, whether simple or multiple, represents the most conventional methodology for analysis. This approach involves regressing crop yield against vegetation indices (VIs) or spectral bands, or combinations thereof with ancillary variables such as weather or soil data. This analysis is sometimes conducted over a specific phenological period. However, linear models assume a linear relationship between predictors and yield, which may be oversimplified in many agricultural and climatic contexts.

Tree-based methods such as Classification and Regression Trees (CART), Random Forest (RF), and Gradient Tree Boosting offer more flexibility. CART is a single decision tree that partitions data by splitting on features (e.g. VIs over time, phenological metrics) to explain yield variability; however, being a single tree it may suffer from high variance [54]. Random Forests mitigate this by averaging many trees; for instance, RF applied with Sentinel-2 data and ancillary predictors has been used for rice yield mapping with good accuracy [55]. Gradient Boosted Regression was successfully used in India to estimate rice yields using time - series of LAI from MODIS (500 m resolution), delivering good spatially explicit estimates and outperforming simpler models [56].

Artificial Neural Networks (ANNs) and related deep learning architectures further extend capability by learning non-linear relationships and interactions among inputs in a flexible manner. ANNs have been shown to outperform linear regression in studies where there are many remote sensing inputs (e.g. multiple vegetation indices, spectral bands, phenological and meteorological variables). For example, in China, remote sensing-based yield estimation of winter wheat using multispectral and hyperspectral data compared RF, GTB, SVR and LSTM: the deep learning model (LSTM) had the lowest RMSE among these [57].

2.6. Classification of Land Use Classes

Land use land cover classification was performed using Sentinel-2 images, which are multispectral images. An image with less than 20 percent cover was selected and used to estimate the area under different land-use classes. The images taken on 14th October 2020 and 29th September 2021 were used to perform land use-land cover classification for *Kharif* 2020-21 and *Kharif* 2021-22 respectively. This classification was performed to obtain the rice-cropped area in the district and to mask the remaining land-use classes in estimating the yield only for rice-cropped areas. The random forest classification method was used for land use classification. The regions of interest (ROI) for different classes used for classification were first identified in Google Earth, converted into KML, and used as a training set for random forest classification.

2.7. Crop Calendar

In our study, we utilized microwave remote sensing data, specifically Sentinel-1 data, to detect changes in soil moisture associated with rice sowing and planting activities, using VH backscatter values. Detecting the transplanting date of rice using Sentinel-1 data involves analyzing changes in backscattering signals over time to identify significant shifts associated with the transplanting process. In this study, we analyzed the time series of Sentinel-1 bands, the VH time series showed a trend close to that of the rice crop calendar. To detect rice sowing dates, we performed a temporal analysis on the Sentinel-1 datasets to identify significant changes in soil moisture patterns over time. Rice sowing activities typically lead to alterations in soil moisture levels, which can be detected through Sentinel-1 imagery because of their sensitivity to surface roughness and soil moisture content. Our analysis involved developing and implementing algorithms tailored to detect rice sowing dates based on observed changes in backscatter values.

The lowest backscatter values of the VH band during the early stages of crop growth seemingly coincided with the transplanting of rice crops with a ± 5-day deviation. These low backscatter values during the period 1st June to 15th August were used to identify the transplanting date. The Sentinel-1 images for the aforesaid periods are stacked, the image with the lowest VH backscatter is identified, and the date of the image is retrieved using GEE-based algorithms. This approach helps to automatically detect the transplanting date of rice crops in Samastipur district, which can be scaled up for any location where the transplanting method is adopted. This automatic detection of transplanting dates across large spatial areas can be helpful for policymakers to identify the extent of sowing in that season. However, uncertainties and limitations are associated with the analysis of rice sowing dates using the Sentinel-1 datasets. Factors such as weather conditions, land cover variability, and data availability may introduce uncertainties into the results, which should be carefully considered and discussed in the context of this study.

2.8. Comparative Analysis of Control and Demo Plots Using Sentinel-1 Derived Indices

The vegetation indices VV/VH and VH/VV were developed using the VH and VV bands of the Sentinel-1 data. Time series of VH, VV, VH/VV, and VV/VH from 1st June to 31st December were developed for each plot and averaged. Then, the Savitzky-Golay smoothing filter was applied to the time-series data to better understand crop progression [73]. Time series and smoothing of the time series were performed using the GEE platform. One-way ANOVA was performed on the demo plot yields against the control plots [74]. Similarly, ANOVA was used for the time series of the VH band to determine differences between the demo and control plots. A Tukey Post Hoc test was used to quantify the difference in the rice crop yields and estimate Tukey's Honest Significant Difference (TSD) using the Real Statistics application, which is used as an add-on to Excel [58]. ANOVA and post-hoc tests were performed at a 0.05% significance level. ANOVA tests were performed on the observed yield of the varieties and VH time series for the demo and control plots. Similarly, the VH time series was averaged across different sowing dates to study the effect of variable sowing dates on crop performance and yield.

2.9. Estimating Crops Yield Synergistically Using Sentinel-1 and Sentinel-2

Crop yield prediction using satellite data is mostly performed at two phenotypical crop growth stages: flowering (F1) and harvesting (F2). However, owing to the lack of cloud-free Sentinel-2 images, prediction was possible only at the F2 stage. Although 30 Sentinel-1 images were available throughout the crop-growing season, the correlation coefficient for most Sentinel-1 bands and indices was less than +/-0.1. Therefore, we integrated Sentinel-1 and Sentinel-2 data to develop yield prediction models. The yield data from rice crops grown in the demo and control plots were used to develop the model. The vegetation indices developed from the Sentinel-1 and Sentinel-2 images were used as proxies for yield. This methodology enables us to estimate crop yields with minimal or no ground-truth data. The yield data of five rice varieties (2082, 6444, 27p31, 27p37, and Rajendra Bhagwati) were used to develop the yield model. The data obtained for the five varieties were split into training (n = 300) and validation (n = 73) datasets; the models were developed using a training dataset and tested on a validation dataset.

2.10. Developing a Yield Prediction Model

The workflow is illustrated in Figure 3 and is described below in a step-wise manner.

1) The averaged time series of vegetation indices (Sentinel-1 and Sentinel-2) was calculated for all the demo and control plots, while excluding the images with cloud cover. The time series of vegetation indices developed for the demo and control plots were pooled and analyzed further.
2) High correlative relationships between explanatory variables (bands and indices) were tested before stepwise regression (SWR) analyses were performed by calculating the variance inflation factor (VIF). The explanatory variables that showed high VIF values were excluded until the remaining explanatory variables had VIF values less than 4. This is primarily used to reduce multicollinearity between the variables.
3) Explanatory variables with a coefficient of correlation of more than 0.2 were selected for use in the model.
4) Furthermore, The SWR model estimates rice yields with more appropriate bands or indices (explanatory variables) The SWR method uses both forward and backward methods to select the explanatory variables that showed the lowest probability values of less than 0.05.
5) After performing SWR, machine learning models, such as CART, random forest (RF), GTB and ANN were developed on the selected variables using the training dataset and validated on the remaining dataset.
6) Hyperparameter tuning plays a crucial role in enhancing a model's accuracy, generalization, and overall performance. To optimize the models, we employed random optimization, a method that samples hyperparameters from predefined ranges rather than exhaustively testing all combinations as in grid search. This approach is particularly efficient for large search spaces with many hyperparameters. During tuning, Root Mean Squared Error (RMSE) was used as the evaluation metric, and the hyperparameter set yielding the lowest RMSE in the training phase was selected. The predictive ability of the models and the effectiveness of model combination approaches were then assessed using the coefficient of determination (R^2). The ANN model was hyperparameter tuned with 0.3 learning rate and three hidden layers, while the RF and GTB model were tuned for hyperparameters with 100 trees and minimum size splits set to 5.
7) The performance of the model was tested by applying measures such as the coefficient of determination (R^2) and the root mean squared error (RMSE). The Sentinel-1 and Sentinel-2 bands and indices are extracted from GEE, and the data were pooled in a Microsoft Excel worksheet. These bands and indices were used as predictor variables in the SWR, ANN, and RF models which were performed outside the GEE platform on the Weka tool, and the models were evaluated using R^2 and RMSE. Then the RF model is performed on the GEE platform and the GEE code for the RF model to predict rice yields of Samastipur district can be accessed (https://code.earthengine.google.com/6c4cf20e8f906cb639a1d31757d12520). The maps in the article were prepared using QGIS 3.30.1 (Hertogenbosch) (https://www.qgis.org/). Origin Pro software (https://www.originlab.co m/origin) version 9.1 was used to represent data in a graphical format [59].

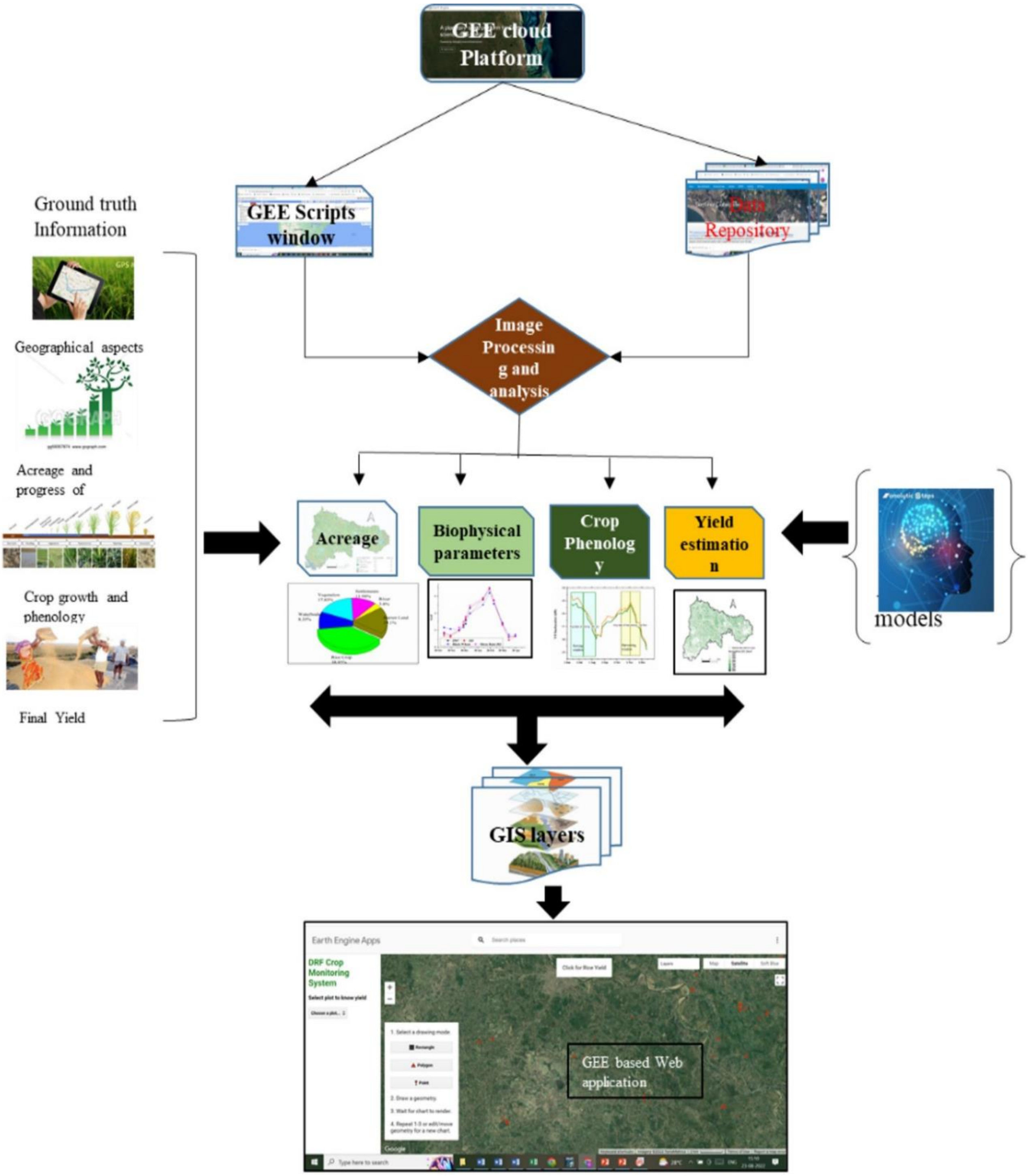

Figure 3. Workflow of the GEE-based web application for crop monitoring and yield estimation, from data processing and analysis to interactive GIS-based visualization.

3. Results

3.1. Summary Statistics of Ground Truth

Table 3 summarizes the ground truth data collected from the demo and control plots for *Kharif* 2020-21 and *Kharif* 2021-22. The trials were conducted on five major rice crop varieties (2082, 6444, 27p31, 27p37, and Rajendra Bhagwati), and data were collected separately from demo and control plots to compare the impact of traditional and improved practices of crop management on crop yields. The duration of rice varieties grown in demo and control plots ranged between 105 days (27p31) and 135 days (Rajendra Bhagwati) for *Kharif* 2020-21; and 103 days (27p31) and 133 days (Rajendra Bhagwati) for *Kharif* 2021-22 (Table 3).

For the *Kharif* 2020-21 the mean rice yield observed in the demo and control plots is 6159.8 kg ha^{-1} and 5766.4 kg ha^{-1}, respectively. The highest mean yield in the demo and control plots was observed for the 27p31 (7920.0 kg ha^{-1}) and Rajendra Bhagwati varieties respectively (6935.0 kg ha^{-1}). The minimum yield observed in the demo and control plots is 3300.0 kg ha^{-1} and 3960.0 kg ha^{-1} for Rajendra Bhagwati and 6444, 27p31 varieties respectively. The mean yield observed for *Kharif* 2021-22 in the demo and control plots is 6722.4 kg ha^{-1} and 6070.6 kg ha^{-1}, respectively. The highest yield in the demo (9600.0 kg ha^{-1}) and control plots (8000.0 kg ha^{-1}) were observed for the 27p31 variety. The minimum yields observed in the demo and control plots were 518.0 kg ha^{-1} and 2400.0 kg ha^{-1} for 27p37 and 27p31, respectively.

3.2. Land Use - Land Cover (LULC) Classification

The area under different land use classes for *Kharif* 2020-21 and *Kharif* 2021-22 are given in Table 4. The classification of Sentinel-2 mean image showed that the area under crop is 731.4 km^2 and 802.4 km^2 during *Kharif* 2020-21 and *Kharif* 2021-22 respectively, which accounts for 25.2 percent and 27.6 percent of the total district area. On average for two seasons, the percentage of area under Rice crop was estimated as 766.9 km^2 (26.4 percent). The area under other crops and vegetation from the Sentinel-2 classified images for *Kharif* 2020-21 and *Kharif* 2021-22 is 1166.2 km^2 (40.2 percent) and 1111.4 km^2 (38.3 percent) respectively. Of all the classes the maximum area is estimated under the class “Other crops and vegetation”. Water bodies in the district accounted for 10 percent and 9 percent of the total area of the district area during *Kharif* 2020-21 and *Kharif* 2021-22 respectively. The LULC image is used to identify the area under different land use classes, and, used as a layer for predicting Rice yields. Classified images of Samastipur district for the seasons *Kharif* 2020-21; and 2021-22 are given in Figure 4. Results show that many of the areas were flooded during *Kharif* 2021-22 leading to the loss of crops in many of the demo and control plots (Figure 4a). From the mean classified Sentinel-2 image we can observe the increase in the barren land by 13.3 percent (Table 4).

Table 3. *Summary Statistics of rice crops grown in demo and control plots during Kharif 2020-21 and Kharif 2021-22.*

Plot	Variety	No. of plots	Date of Sowing (mean)	Crop Duration (days)	Yield kg ha^{-1}		
					Mean	Max	Min
Kharif 2020-21							
Demo	2082	2	21-06-2020	115	6600	7260	5940
	27p31	9	17-06-2020	105	6442	7920	4875
	27p37	14	19-06-2020	121	5762	6600	5016
	6444	14	20-06-2020	124	6385	7260	4620
	Rajendra Bhagwati	3	29-06-2020	135	5610	6930	3300
	Mean	42	21-06-2020	120	5766.4	7920	3300
Control	2082	3	13-06-2020	116	5500	5940	5280
	27p31	8	24-06-2020	106	5473	6303	3960
	27p37	18	20-06-2020	117	5168	6600	4500
	6444	10	19-06-2020	120	5756	6600	4960
	Rajendra Bhagwati	1	07-07-2020	132	6935	6935	6935
	Mean	40	22-06-2020	118.2	5766.4	6935	3960
Kharif 2021-22							
Demo	2082	7	29-06-2021	114	7041	7800	4800
	27p31	62	11-07-2021	106	6239	9600	2667
	27p37	58	02-07-2021	116	6500	8400	518
	6444	136	12-07-2021	118	5990	8800	2560

Plot	Variety	No. of plots	Date of Sowing (mean)	Crop Duration (days)	Yield kg ha^{-1}		
					Mean	Max	Min
	Rajendra Bhagwati	17	17-06-2021	130	7842	8000	7000
	Mean	280	02-07-2021	116.8	6722.4	9600	518
	2082	4	08-07-2021	116	5920	7200	5120
	27p31	13	17-07-2021	103	6135	8000	2400
	27p37	14	04-07-2021	119	6021	7067	5024
Control	6444	17	07-07-2021	126	5877	7600	2596
	Rajendra Bhagwati	1	18-06-2021	133	6400	6400	6400
	Mean	45	04-07-2021	120.3	6070.6	8000	2400

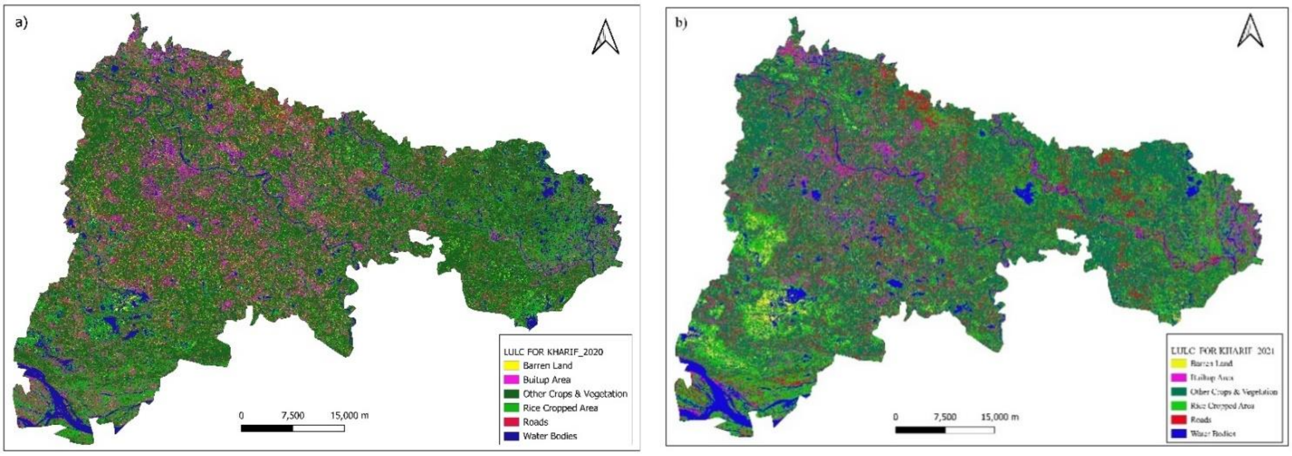

Figure 4. *Sentinel-2 based land use land cover classified images for a) Kharif 2020-21 and b) Kharif 2021-22. Maps were prepared using QGIS 3.42.0 (https://qgis.org/).*

Table 4. *Area under land use land cover classes estimated using Sentinel-2 data for Kharif 2020-21 and Kharif 2021-22.*

LULC classes	2020-21		2021-22		Mean	
	Area (km^2)	Area (%)	Area (km^2)	Area (%)	Area (km^2)	Area (%)
Barren land	137.5	4.7	71.3	2.5	104.4	3.6
Built-up	132.3	4.6	167.3	5.8	149.8	5.2
Other crops	1012.6	42.4	973.8	33.5	1103.4	38.0
Rice Crop	1102.1	30.5	906.0	31.2	895.7	30.8
Vegetation	456.4	15.7	726.4	25.0	591.4	20.4
Water Bodies	61.1	2.1	57.0	2.0	59.1	2.0
Mean	2902.0	100.0	2902.0	100.0	2902.0	100.0

3.3. Crop Calendar

From the graphs presented in Figure 5, it is evident that the vertical horizontal dual-polarized band (VH) is more related to the crop calendar and growth of rice crops than other bands and indices. The average date of sowing observed in the Samastipur rice crop is 25th June 2020, and 10th July 2021 *Kharif* 2020-21 and *Kharif* 2021-22. However, transplanting was performed 21-30 days after sowing, which could be during the 2nd week of July 2020 and the 1st week of August 2021, which is evident from the VH time series in Figure 5. The VH increases with an increase in the vegetative growth of the crop and starts to decline after the crop reaches maturity when the leaves begin to wither. The VH time series is indicative of the vegetative growth peaks during the last week of September to the 1st week of October for *the Kharif* 2020 crop, whereas for *Kharif* 2021, the peak is observed during the 2nd week of October to 1st week of November. The difference in the sowing time of rice crops between *Kharif* 2020-21 and *Kharif* 2021-22 is evident from the VH time series data.

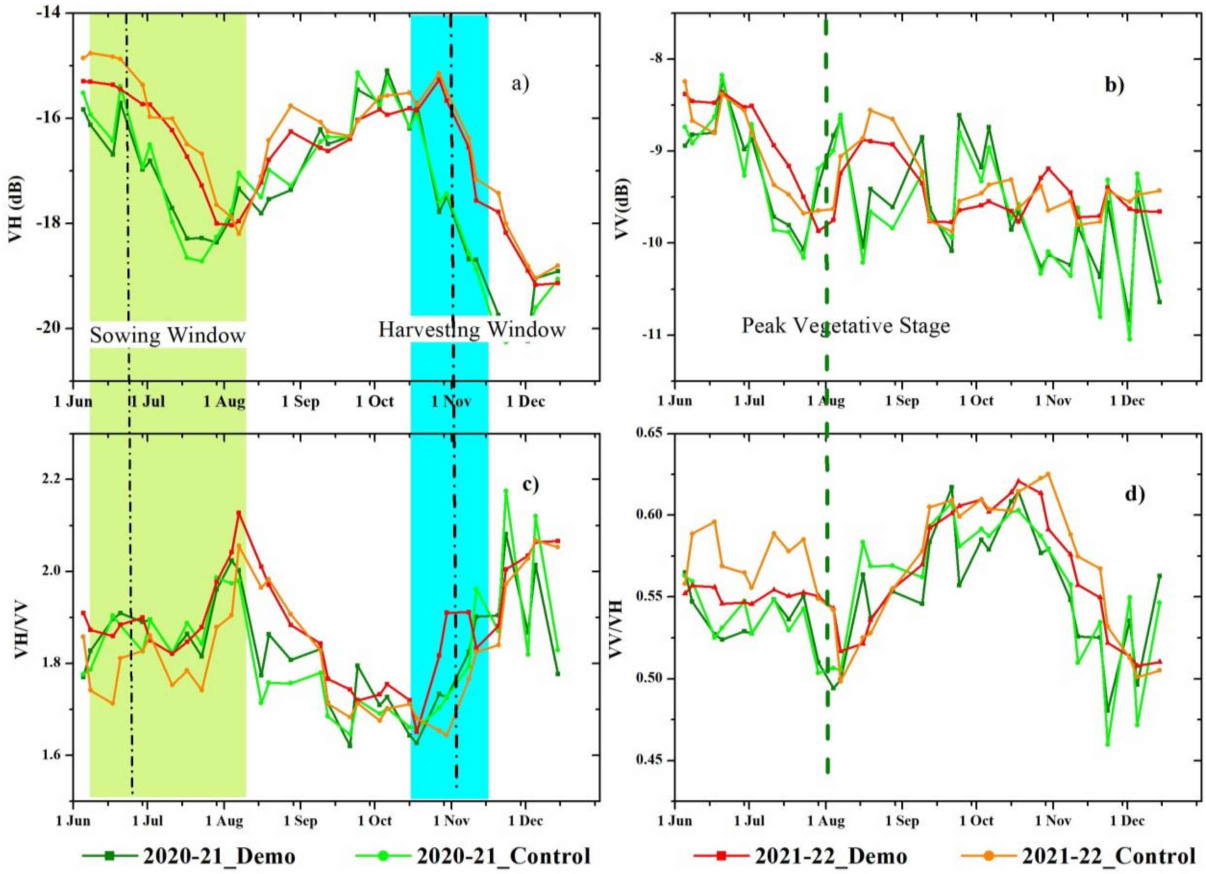

Figure 5. *Sentinel -1 derived estimates a - b) an average of VH and VV backscatter measurements over the demo and control plots. c - d) Average of VV/VH and VH/VV indexes over demo and control plots for rice crops for Kharif 2020-21 and Kharif 2021-22. Graphs were prepared using Origin Pro v 9.1 software (https: //www.originlab.com/origin).*

3.4. Comparison Between Control and Demo Plots Using Sentinel-1 Estimates

Variety-wise ANOVA performed for VH band backscatter values between demo and control plots is presented in Table 5. For the season *Kharif* 2020-21, results show that the average VH values for demo and control plots are -17.3 dB and -17.18 dB, respectively. The VH values for demo plots ranged from -16.7 dB (2082) to - 18.0 dB (27p31 and Rajendra Bhagwati), while the VH values for control plots ranged from - 16.1 dB (2082) to - 18.5 dB (Rajendra Bhagwati). ANOVA of the time series of VH backscatter values obtained for different varieties grown under demo and control plots show significant differences between the growth patterns of demo and control plots in 2082, 6444, and 27p37 at a 95 percent level of confidence (indicated with single asterisk (*)).

For 27p31 and Rajendra Bhagwati, the time series of VH of demo and control plots were not significantly different. The ANOVA observed *Kharif* 2020-21 rice yield, and the critical difference (CD) value of 456 kg ha^{-1} shows that there is a significant difference in yields of demo and control plots of all the five varieties at a 95 percent level of confidence.

Similarly, for *Kharif* 2021-22, average VH values for demo and control plots are -16.58 dB and -16.54 dB, respectively. The VH values for demo plots ranged from -16.1 dB (Rajendra Bhagwati) to - 16.8 dB (2082), while the VH values for control plots ranged from - 16.1 dB (27p37) to - 17.2 (Rajendra Bhagwati). ANOVA of the time series of VH backscatter values obtained for different varieties grown under demo and control plots show a significant difference between the growth patterns of demo and control rice plots in 27p31 and Rajendra Bhagwati at a 99 percent level of confidence (indicated with double asterisk **). For 2082 and 27p37, the demo and control plots are significantly different at a 95 percent level of confidence. ANOVA of the VH time series shows a significant difference in the control and demo plots of 4 rice varieties, viz., 2082, 27p31, 27p37, and Rajendra Bhagwati. ANOVA of *Kharif* 2021-22 yield and based on CD value of 228 kg ha^{-1} it is observed that there are significant differences in yields of demo and control plots of 2082, 27p37, and Rajendra Bhagwati varieties ($p<0.05$).

3.5. Plot-wise Comparison of Demo and Control Plots

In the previous section, we compared the average yields of varieties grown in demo and control plots. However, it is important to see if we can discriminate the demo and control plots at each plot level (field scale). For this purpose, we have selected one demo and one control plot for each variety for each season. ANOVA was performed on a VH time series of selected plots to check if there was any significant difference between the demo and control plots. Table 6 presents the details of selected demo and control plots for *Kharif* 2020-21 and *Kharif* 2021-22 such as plot-ID, area of the selected plot, sowing date of rice crop in that plot, yield and the difference in yield between demo and control plots along with ANOVA, a p-value of VH time series between demo and control plots for each variety. The sowing date for varieties 2082, 27p31, 27p37 and 6444 varieties during *Kharif* 2020-21 is 1st June, 28th June, 12th June and 5th June, the sowing/transplanting of the crop in control and demo plot is considered simultaneously to be able to study the effect of improved management practices. However, in Rajendra Bhagwati due to flooding, many plots got submerged leading to the loss of crops. So, to substantiate the loss we compared one demo plot with another control plot (SRD12 with SRC8). For the Rajendra Bhagwati variety, the crop in the demo plot was sown on 30th June while for the crop in the control, plot was sown on 7th July. It is observed from ANOVA of VH time that there are significant differences between selected demo and control plots of 27p31 and 6444 varieties. The yield difference in the demo plots compared to control for 2082, 27p31, 27p37, 6444, and Rajendra Bhagwati was 1320 kg ha^{-1}, 474 kg ha^{-1}, 990 kg ha^{-1}, 0 kg ha^{-1} and -335 kg ha^{-1}. It is to be noted that for the Rajendra Bhagwati variety, the yield in the demo plot is less than the yield in the control plot. The results from the VH time series and yield values agree for all varieties except for Rajendra Bhagwati. The seasonal average of the VH index image of the demo and control plots and the VH time series graphs of demo and control plots for each variety are given in Figure 6 for *Kharif* 2020-21. From the time series, the phenological stages could be differentiated in 27p31, 27p37, and 6444 varieties. However, for 27p37 and Rajendra Bhagwati the phenological stages could not be differentiated but time series could differentiate the delay in sowing in the Rajendra Bhagwati control plot.

Table 5. *Average VH index for each variety and p-value calculated from ANOVA and its significance.*

Variety	Yield (kg ha^{-1})			VH (dB)		p-value	Significance
	Demo	Control	Difference	Demo	Control		
Kharif 2020-21 (CD@0.05 = 456 kg ha^{-1})							
2082	6600	5499.9	1100**	-16.7	-16.1	0.02	*
6444	6384.6	5755.8	629**	-16.8	-17.1	0.01	*
27p31	6441.9	5472.9	969**	-18	-17.7	0.35	
27p37	5761.8	5168.4	1325**	-17	-16.5	0.03	*
Rajendra Bhagwati	5610	6935	1325**	-18	-18.5	0.45	
Mean	6159.6	5366.4	793**	-17.3	-17.2	0.63	
Kharif 2021-22 (CD@0.05 = 228 kg ha-1)							
2082	7041.1	5920	1121**	-16.8	-16.4	0.05	*
6444	5990.3	5877.4	113	-16.7	-16.8	0.05	**
27p31	6239.4	6135.1	104	-16.7	-16.2	0.01	

Variety	Yield (kg ha^{-1})			VH (dB)		p-value	Significance
	Demo	Control	Difference	Demo	Control		
27p37	6500.4	6021.6	479**	-16.6	-16.1	0.02	*
Rajendra Bhagwati	7841.7	6400	1442**	-16.1	-17.2	0	**
Mean	6722.6	6070.8	652**	-16.6	-16.5	0	**

* Indicates a significant difference at 0.05 level of confidence
** Indicates a significant difference at 0.01 level of confidence

The sowing dates for varieties 2082, 27p31, 27p37 and 6444 during *Kharif* 2021-22 in demo plots were 25th June, 15th July, 19th July, 8th July and 18th June, and for control plots on 25th June, 1st July, 18th July, 8th July and 20th June respectively (Table 6). The sowing of control plots during *Kharif* 2021-22 was taken up simultaneously or with a lag of 1 or 2 days, except for 27p31, where there was a difference of 15 days between the demo and control plot sowing dates. ANOVA of the VH time series shows significant differences between the selected demo and control plots of 2082, 27p31 and Rajendra Bhagwati varieties. The yield difference in the demo plots compared to control for 2082, 27p31, 27p37, 6444 and Rajendra Bhagwati was 2000 kg ha^{-1}, 2400 kg ha^{-1}, 300 kg ha^{-1}, 72 kg ha^{-1} and 1109 kg ha^{-1}. In all demo plots, the yield recorded was higher than that of the corresponding control plot. The results from the VH time series and yield values agree for all varieties, showing a yield difference of >1000 kg ha^{-1}, and the VH time series of the control and demo plots were found to be significantly different. The seasonal average of the VH index image of the demo and control plots and the VH time-series graphs of the demo and control plots for each variety are shown in Figure 7 for *Kharif* 2021-22.

However, for 6444 and Rajendra Bhagwati, the crop calendar could not be differentiated, but the time series could differentiate the sowing delay in the Rajendra Bhagwati control plot. The color mapping graph in Figure 8 indicates the time series of VH backscatter from 1st May 2021 to 31st October 2021 as influenced by the variable dates of sowing. Different colors on each of the time series indicate the range of VH backscatter values. The legend shows a color scale indicating the value of the VH backscatter. Higher values of VH indicate a better crop, while lower values indicate a poor-performing crop. The color map indicates that in the early sown crops (1st and 2nd weeks of June) and late sown crops (4th week of July and 1st week of August), the VH backscatter is lower compared to the crop sown in the 3rd week of June to 3rd week of July. The VH value for crops sown in the 1st week of June and the 1st week of August is lower than -19.0, which suggests less vegetative growth when compared to crops sown on other dates. This lower vegetative growth may consequently impact in lowering crop yields. The comparative study of the VH time series and the values of the VH backscatter can help study crop performance under various climatic conditions.

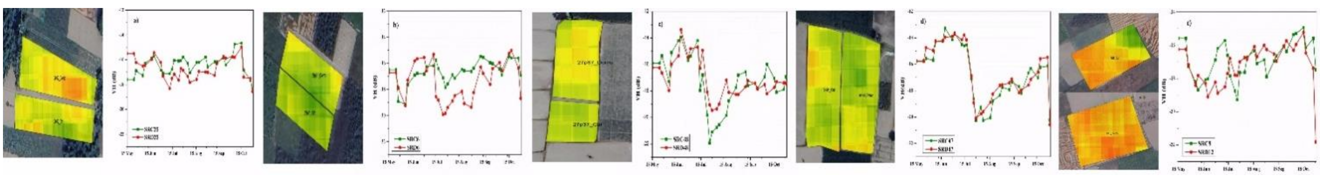

Figure 6. *Plot-wise comparison of demo and control plots with the VH time series for Kharif 2020-21. The images in this figure were processed and downloaded from the GEE platform (https://code.earthengine.goog le.com/), and graphs were prepared using the Origin Pro v 9.1 software (https://www.originlab.com/origin).*

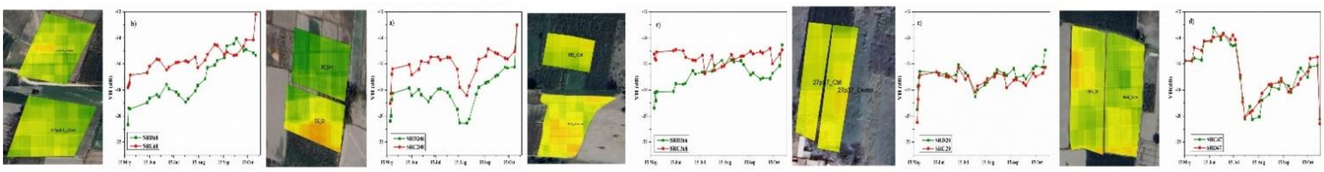

Figure 7. *Plot-wise comparison of demo and control plots with the VH time series for Kharif 2021-22. The images in this figure were processed and downloaded from the GEE platform (https://code.earthengine.goog le.com/), and graphs were prepared using the Origin Pro v 9.1 software (https://www.originlab.com/origin).*

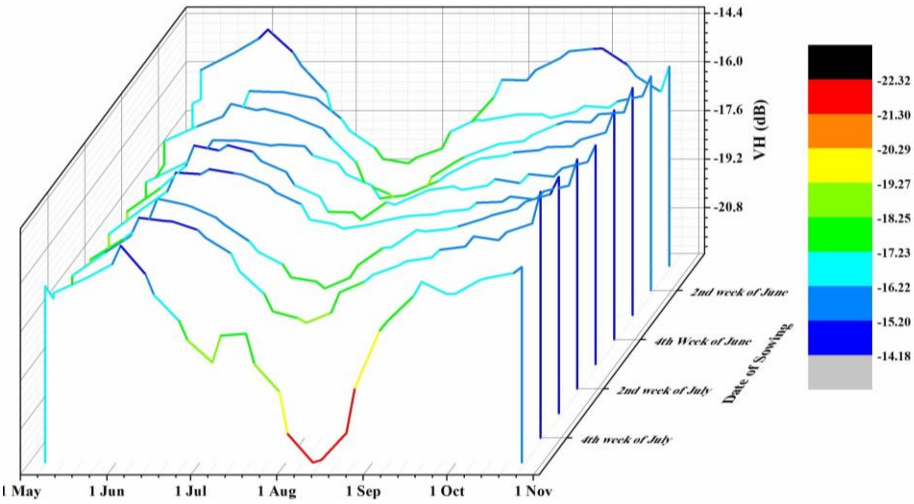

Figure 8. 3D color graph indicates the effect of different sowing dates on crops according to Sentinel-1 VH band time-series. Graphs were prepared using the Origin Pro v 9.1 software (https://www.originlab.com/origin).

Table 6. Plot-wise comparison and ANOVA on VH time series and the p-value (significance) estimated between control and demo plots in rice crop during Kharif 2020-21 and Kharif 2021-22.

Variety	PlotID	Plot	Area (m^2)	Sowing Date	Yield (kg ha^{-1})	Yield Δ	(p-value)
Kharif 2020-21							
2082	SRC25	Control	1632	01/06/2020	5940	1320	0.05*
	SRD25	Demo	943	01/06/2020	7260		
27p31	SRC6	Control	999	28/06/2020	5292	474	0.56
	SRD6	Demo	892	28/06/2020	5766		
27p37	SRC48	Control	670	12/06/2020	5610	990	0.03*
	SRD48	Demo	369	12/06/2020	6600		
6444	SRC47	Control	1759	05/06/2020	6600	0	0.41
	SRD47	Demo	1824	05/06/2020	6600		
Rajendra Bhagwati	SRC8	Control	295	07/07/2020	6935	-335	0.001**
	SRD12	Demo	2777	30/06/2020	6600		
Kharif 2021-22							
2082	SRC208	Control	1027	25/06/2021	5200	2000	0.001**
	SRD208	Demo	521	25/06/2021	7200		
27p31	SRC68	Control	2507	15/07/2021	4800	2400	0.005**
	SRD68	Demo	1359	01/07/2021	7200		
27p37	SRC20	Control	1387	19/07/2021	6100	300	0.51
	SRD20	Demo	1335	18/07/2021	6400		
6444	SRC7	Control	1363	08/07/2021	6160	72	0.94
	SRD7	Demo	1441	08/07/2021	6232		
Rajendra Bhagwati	SRC368	Control	2112	18/06/2021	6400	1109	0.01*
	SRD366	Demo	1421	20/06/2021	7509		

3.6. Estimating Crop Yields Using both Sentinel-1 and Sentinel-2

Table 7 evaluates the performance of different statistical models in estimating a rice yield using Sentinel-1 and Sentinel-2-derived indices, along with the Date of Sowing (DOS). The indices are temporally specific, as indicated by the numbered suffixes denoting the image acquisition dates. Among the models, Gradient Tree Boosting (GTB) and Random Forest (RF) deliver the highest accuracy, with both showing strong calibration performance (R^2 = 0.96). GTB maintains a slight edge in validation (R^2 = 0.77, RMSE = 551.04), suggesting better generalization to unseen data. These ensemble learning methods are especially well-suited for handling the complex, nonlinear relationships present in multi-temporal satellite imagery.

Linear Regression and CART provide moderate performance, suggesting they capture only a limited portion of the variance in the data. The poor performance of the Artificial Neural Network (ANN), particularly during validation (R^2 = 0.33, RMSE = 970.83), indicates potential issues such as overfitting, inadequate training data, or suboptimal architecture. Overall, the results underscore the effectiveness of ensemble tree-based models in leveraging temporal and spectral patterns from Sentinel imagery for agricultural prediction tasks.

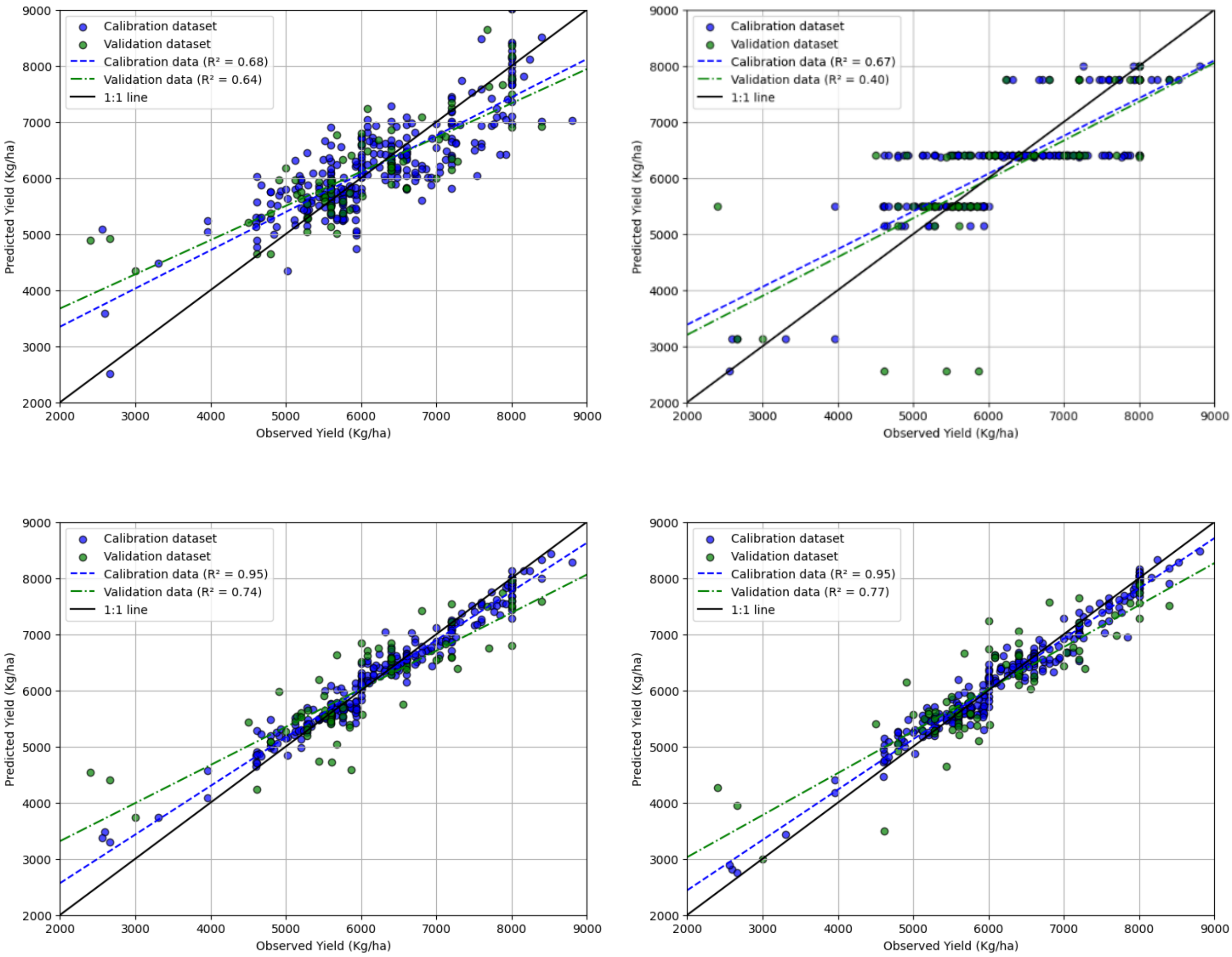

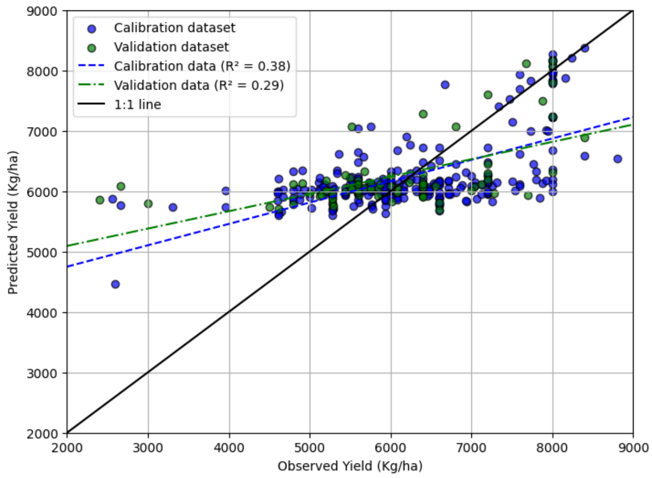

Figure 9. *Scatterplots of observed and predicted Rice yields in Samastipur district for training (n=298) and validation (n=75) datasets using Linear Regression, CART, RF, GTB and Artificial Neural Networks (ANN) statistical models. Graphs prepared using the Origin Pro v 9.1 software (https://www.originlab.com/origin).*

Table 7. *Statistical models developed for yield prediction at the F2 stage of rice crops using remote sensing-based indices, R^2, and RMSE calculated between actual and predicted yields.*

Model	Variables	Bands	R^2 (Cal)	RMSE (Cal) kg ha^{-1}	R^2 (Val)	RMSE (Val) kg ha^{-1}
Linear	NDVI232, EVI248, B12_293, B3_293, B4_293, REIP_248, REIP_293, VH/VV_232, VH/VV_241, VH/VV_277, VV_211, DOS	B4, B8, B3, B4, B5, B6, B7, B8, B12, VH, VV	0.68	595.44	0.65	687.59
CART			0.67	603.77	0.49	889.08
RF			0.96	232.90	0.74	591.66
GTB			0.96	227.91	0.77	551.04
ANN			0.39	828.53	0.33	970.83

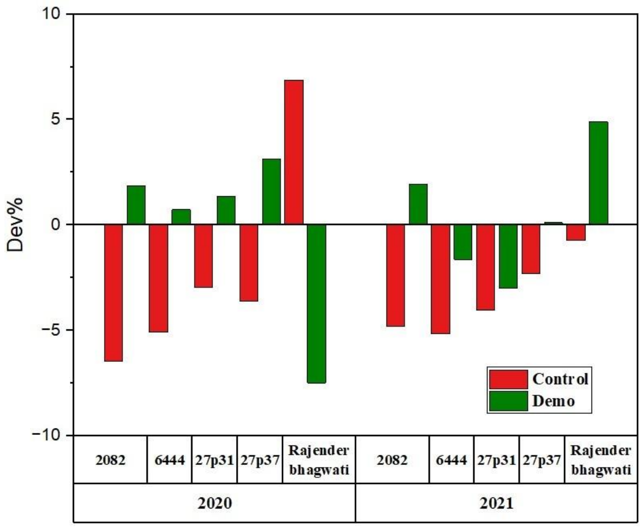

Figure 10. *Deviation percentage between yields of demo and control plots for observed and estimated yield data for Kharif 2020-21 & 2021-22. Graph prepared using the Origin Pro v 9.1 software (https://www.originlab.com/origin).*

3.7. Comparison of Estimated Rice Yields in Control and Demo Plots

The validated GTB model was used to estimate the yields of the rice crop varieties, and the yields of the control and demo plots were compared. The deviation percentage between yields of demo and control plots was calculated for observed and estimated yield data, as shown in Figure 10. The estimated yields for the control and demo plots using the GTB models for the five rice varieties are presented in Figure 11. The deviation percentage was estimated between observed and estimated yields of demo and control plots to validate the performance of the remote sensing-based crop yield model and identify the differences between the improved and traditional management practices. The average deviation percentages of the estimated yield from the observed yield for *Kharif* 2020-21 and *Kharif 2021*-22 were 3.9 percent and 2.8 percent, respectively. The percentage deviation of estimated yields from the observed yield for *Kharif* 2020-21 was found to be higher for the Rajendra Bhagwati variety (6.9 percent) and lowest for the 27p31 variety (-2.9 percent) among the control plots. Similarly, the deviation percentage for the demo plots was higher for the Rajendra Bhagwati variety (-7.5 percent) and lowest for the 6444 variety (0.73 percent).

The deviation percentage of estimated yields from the observed yield for *Kharif* 2021-22 was found to be higher for the 6444 variety (-5.2 percent) and lowest for the Rajendra Bhagwati variety (-0.72 percent) among the control plots. Similarly, for the demo plots, the deviation percentage was found to be higher for the Rajendra Bhagwati variety (4.9 percent) and lowest for the 27p37 variety (0.11 percent) (Figure 10).

For *Kharif* 2020-21 the RF model estimated yield for all varieties in control plots ranging between 6609.0 (6444) and 4525.5 (27p37) with an average yield of 5648.6 kg ha^{-1} for all varieties. For demo plots, the estimated yield ranged between 7097.8 kg ha^{-1} (2082) and 4323.5 kg ha^{-1} (Rajendra Bhagwati) with an average yield of 6020.1 kg ha^{-1} for all varieties.

For all varieties, the yields of demo plots were found to be higher than the rice varieties grown in control plots, except for the Rajendra Bhagwati variety, where the control plot (6458.6 kg ha^{-1}) yields on average were higher than those of the demo plots (5756.5 kg ha^{-1}) (Figure 11). For *Kharif* 2021-22 the GTB model, estimated yield for all varieties of control plots ranged between 7225.1 kg ha^{-1} (27p31) and 3421.6 kg ha^{-1} (27p31) with an average yield of 6073.3 kg ha^{-1} for all varieties. The estimated yield for all varieties of demo plots ranged between 8692.7 kg ha^{-1} (27p31) and 3825.7 kg ha^{-1} (6444) with an average yield of 6320.5 kg ha^{-1} for all varieties. For all the varieties, the yields of demo plots were found to be higher than the yield of rice varieties grown in control plots, except for 6444 varieties where the control plot (6095.4 kg ha^{-1}) yields on average were higher than those of the demo plots (6007.6 kg ha^{-1}) (Figure 11b).

3.8. Interactive Web Interface for Crop Monitoring and Crop Yield Prediction

A web-based interactive platform to monitor crop status and estimate yield from remote sensing-based vegetation indices was developed using the GEE Manage Apps option. Users can create and implement web apps using the Earth Engine JavaScript API to facilitate exploration and querying of datasets and results. This allows those without Earth Engine access to explore data and derived datasets without using the Code Editor and provides control over how users interact with it. The Sentinel-1-based VH time series, deviation in the current VH index of the selected field from the previous VH index, normalized differential vegetation index (NDVI) time series, and yield predicted for *Kharif* 2020-21 and *Kharif* 2021-22 for the selected field can be accessed through this interactive web application. The user needs to select the area of interest, year, and viewing parameters. This app estimates crop status, transplanting date, and yield for the selected year and season. This application is scalable across time and space; however, it requires validation for its accuracy and can be trained with more ground-truth information to achieve the desired outcomes. The Rice crop Monitoring Tool can be accessed @ https://ee-icrisat.projects.earthengine.app/view/rice-crop-monitoring-tool-icrisat.

4. Discussion

4.1. Land Use - Land Cover (LULC) Classification

According to a report published by the Directorate of Economics and Statistics, Department of Planning and Development, Government of Bihar, the rice-cropped area in Samastipur district is 864.05 km^2 which is 29.8 percent [60]. The rice-cropped area reported by the Directorate of Economics and Statistics is close to the rice-cropped area estimated by Sentinel-2 data for *Kharif* 2020-21, which is 885.5 km^2 (30.5 percent) with less than 5 percent deviation. The area under each land use class was matched with the European Space Agency's (ESA) World Cover 10 m product, which provides a global land cover map at 10 m resolution based on Sentinel-1 and Sentinel-2 data [78]. Other crops grown during *Kharif* in Samastipur include maize and red grams. For *Kharif* 2021-22, it is observed that the area under these crops decreased by 259.1 km^2 and the area under other vegetation types increased by 270 km^2 in comparison with *Kharif* 2020-21. This could be due to late sowing in the district caused by the late onset of monsoon rainfall. The increase in the area under the other vegetation class can mainly be attributed to less rainfall received during 2021 (1236 mm) compared with 2020 (1863 mm) [61]. Lower rainfall during *Kharif* 2021-22 led to less sown area under rice and other crops, which in turn led to the growth of spurious vegetation. Amongst all the classes, the maximum area (38.0 percent) on average is estimated under the class "Other crops". Water bodies in the district accounted for 2.1 percent and 2 percent of the total district area during *Kharif* 2020-21 and *Kharif* 2021-22 respectively. The LULC image was further used to identify the area under different land-use classes and as a layer for predicting rice yields. According to the report, the total district area is 2904 km^2; however, due to clipping of the classified Sentinel-2 raster image using a Shapefile, some pixels may have been lost, resulting in a difference of 2 km^2 between our estimate and the reported area of the district with the total area under LULC classes in Table 4. However, these estimates may not be annually consistent.

4.2. Crop Calendar

The higher the VH value, the higher the vegetation growth; however, water in the field reduced the VH value. The decrease in the VH value shortly after the onset of the monsoon (1^{st} week of June) can be attributed to rainfall and the removal of weeds or other vegetation during land preparation. The low backscatter values are most likely related to specular reflection of the irrigated water surface [62, 63]. The increase in VH value from the second fortnight of July was due to the transplanting which was done 21-30 days after nursery sowing (the observed dates of sowing are given in light green color, and the line intercepting the blue stretch indicates the mean date of sowing).

The lowest VH values indicated less or no vegetation due to land preparation, specifically puddling. Low VH values were used to identify sowing date from 1st June to 15th August. VV indicates the presence of water and water content in the crops or soil; the lower the value of VV, the higher the water content in the satellite image. The time series of VV of the demo and control plots showed an increase in the VV value, indicating a peak in the 3rd week of August, which coincides with the peak vegetative growth stage of the rice crop. During the heading stage, carbohydrates assimilated in the leaves are transported to the panicles, leading to leaf senescence and resulting in the reduction of vegetative growth. The increase in vegetative growth from transplanting to the peak vegetative stage and the subsequent decrease due to heading was evident in the time series of VV (Figure 5). The team collected data on the date of sowing and harvesting, but the peak vegetative stage is a probable indication from the VV time series. The maximum value of VV could be due to vegetation and less soil, which in turn leads to more scattering, and the signal received in the VV direction indicates the presence of erect or upright leaves [64]. During the maturity stage, rice plants begin to senesce, and biomass gradually decline as grains develop which is characterized by a decline in the VH backscatter coefficient. The decrease in VH is linked to the drying and hardening of the plant structure, as well as a decrease in the water content inside plant tissues. However, more ground-truth data would lead to increased discerning capability.

The color mapping graph in Figure 8 indicates the time series of VH backscatter from 1st May 2021 to 31st October 2021 as influenced by the variable dates of sowing. Different colors in each time series indicate the range of the VH backscatter values. The legend shows the color scale that indicates the value of the VH backscatter. Higher VH values indicate a better crop, whereas lower values indicate a poor-performing crop. The color map indicates that in the early sown crops (1st and 2nd weeks of June) and late sown crops (4th week of July and 1st week of August), the VH backscatter was lower compared to the crop sown in the 3rd week of June to 3rd week of July. The VH value for crops sown in the 1st week of June and the 1st week of August is lower than -19.0, which suggests slow vegetative growth when compared to crops sown on other dates. This lower vegetative growth may consequently result in lower crop yields. A comparative study of the VH time series and the values of VH backscatter can help study crop performance under various climatic conditions.

4.3. Comparison Between Control and Demo Plots Using Sentinel-1 Estimates

Based on one-way ANOVA for demo and control yields (ground truth data) and from critical difference values calculated (456 kg ha^{-1} and 228 kg ha^{-1} for *Kharif* 2020-21 and *Kharif* 2021-22 respectively) it was observed that there is a significant difference between the yields demo and control plots for all five varieties during *Kharif* 2020-21 and for 2082, 27p37 and Rajendra Bhagwati during *Kharif* 2021-22. This indicates that improved management practices have a significant effect on rice crop yields. The ANOVA performed over the VH time series of demo and control plots for the rice varieties according to *Kharif* 2020-21 and *Kharif* 2021-22 indicated that there was a significant difference in the time series of VH backscatter values for 2082, 6444, and 27p37 during *Kharif* 2020-21 and for four varieties except 6444 during *Kharif* 2021-22.

The recommended seed treatment, seedling age for transplanting, application of fertilizers in the nursery, spacing between crops and rows, dosage and timing of nutrients, and other recommendations seemed to have a direct effect on the crop and soil (Table 1). The impact of improved seed treatment, nursery management, transplanting age of seedlings, and nutrient management was observed in all varieties of *Kharif* 2020-21 and four rice varieties viz. 2082, 27p31, 27p37, and Rajendra Bhagavathi during *Kharif* 2021-22, while for 6444, the effect of improved management practices was not significant during *Kharif* 2021-22. The difference in the *Kharif* 2020-21 yield between the control and demo plots was not reflected in the VH time series data for varieties 27p31 and Rajendra Bhagwati. The VH time series for *Kharif* 2021-22 differentiated the control and demo plots for the three varieties 2082, 27p37, and Rajendra Bhagwati, in agreement with the yield difference. This differential response of varieties can be attributed to rainfall and flooding in the plots, confirming the differential response of varieties to the treatments.

4.4. Estimating Crop Yields Using both Sentinel-1 and Sentinel-2

Many studies have used Sentinel-1 time series data to estimate rice yields [63, 65] and also to differentiate the early and late sown crops [28] and differentiate irrigated and non-irrigated rice crops [66]. These studies have indicated that remotely sensed data can be used to study the impact of different management practices on crop growth and yield.

Integrating Sentinel-1 and Sentinel-2 data for developing a rice crop monitoring system has proved to be an effective tool for monitoring crop conditions or estimating crop yields even under cloudy situations [67-69]. The evaluation of five statistical models for rice yield estimation: Linear Regression, CART, Random Forest (RF), Gradient Tree Boosting (GTB), and Artificial Neural Network (ANN) using Sentinel-1 and

Sentinel-2 indices and the Date of Sowing (DOS) provides important insights into model behavior for agricultural prediction tasks.

Generally, gradient tree boosting and random forest regression models have given more reliable crop yield estimates than linear, CART and neural network regression as these models have unique characteristics such as: (i) it incorporates the interaction between predictors; (ii) it is based on ensemble learning theory, which allows it to learn both simple and complex problems; (iii) these models does not require much fine-tuning of its hyper-parameters as compared to deep learning techniques (ANN). However, ANN requires many dependent variables and a huge dataset for developing several hidden layers, which in turn provide final estimates [70-72]. The difference between the average estimated yields of demo and control plots for all the varieties is more than a critical difference of 228 kg ha^{-1} (estimated using the Tukey Post Hoc test in Table 5. However, for 6444 (-262 kg ha^{-1}) and 27p31 (237 kg ha^{-1}) the CD was closer to 228 kg ha^{-1}. In the case of observed yields, ANOVA indicated that there is no significant difference between demo and control plots for these two varieties (6444 and 27p31).

The mean deviation percentage for all the varieties in control and demo plots for the two seasons was found to be less than 5 percent indicating that the model performance is good and upon more training and validation, this model can be scaled up to more number of districts making the yield prediction estimates more accurate and less time consuming similar to the study done earlier by Arumugam et al. (2021) [56]. The use of machine learning models in combination with remote sensing data for predicting rice crop yields was demonstrated in several studies [38, 67, 69]. The range of estimated yields in the demo and control for two seasons for five rice varieties indicated that the model differentiated the yields of demo and control plots as observed from the actual ground truth data. From this, it is inferred that a remote sensing-based yield model for rice crops can detect the difference between the crop grown with improved management practices and the crop grown with traditional management practices. Many studies have reported the use of Sentinel-1 and Sentinel-2 data for providing timely and accurate yield estimates for planning and policymaking for Governments and for insurance companies for reliable and timely disbursement of insurance to farmers [16, 73-75].

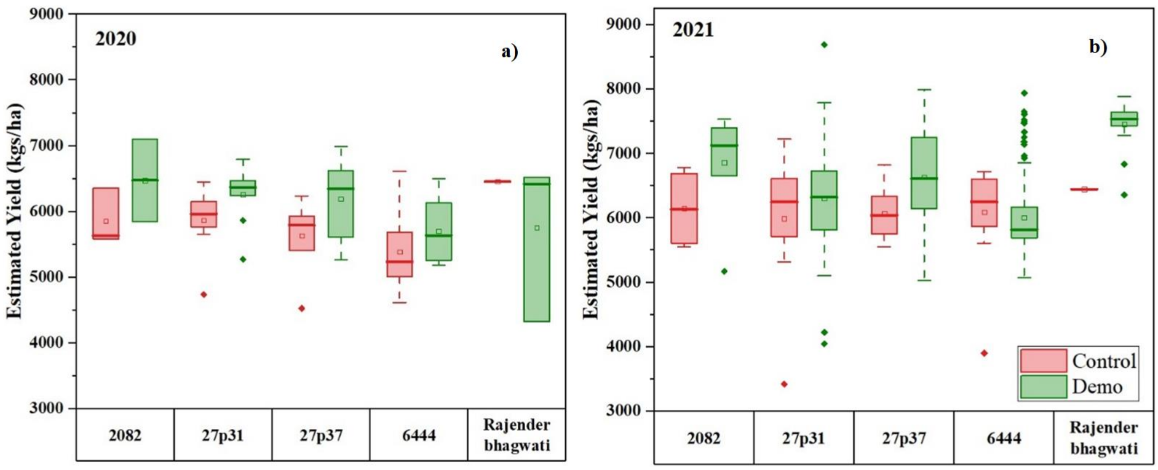

Figure 11. *Estimated yields for control and demo plots for the five Rice varieties for a) Kharif 2020-21 and b) Kharif 2021-22 using GTB model. Graph prepared using the Origin Pro v 9.1 software (https://www.originlab.com/origin).*

4.5. Interactive Web Interface for Crop Monitoring and Crop Yield Prediction

The development of a web-based interactive platform for monitoring crop status and estimating yield from remote-sensing-based vegetation indices represents a significant advancement in agricultural monitoring. The scalability of the platform across time and space indicates its potential for applications in various regions and periods. Its accuracy relies on thorough validation and training with extensive ground-truth information. More comprehensive datasets and rigorous validation studies are needed to enhance its reliability and predictive power [76, 77]. However, this application has a few limitations, including its geographical scope being limited to a specific region, its focus on rice yield estimation alone, and its small dataset. Additional validation and expansion of the dataset are required to enhance the robustness and reliability of the app.

4.6. Limitations of the Study

Nevertheless, a few shortcomings must be addressed with additional research and development:

1. The planting date estimated using the Sentinel- 1 VH time series is not applicable for directly seeded rice or

aerobic rice.

2. Further validation and training are required for scaling up.
3. Farmers require instruction and training to use web applications.
4. The estimated yield was based only on satellite-based vegetation indices. Weather and soil information can increase the accuracy of the estimated yield.

Despite its numerous advantages, GEE also has a few limitations, including interface complexity, requiring a steep learning curve for users unfamiliar with remote sensing and geospatial analysis [78]. Furthermore, the processing capabilities of GEE are sometimes constrained by limitations on computational resources, leading to longer processing times for large datasets. The advantages of adopting GEE for rice crop monitoring outweigh its drawbacks, making it a valuable tool in precision agriculture and sustainable food production. Several studies have emphasized the limitations of temporal and spatial resolution in open-source satellite imagery. They concluded that while satellites such as Sentinel-2 and Landsat provide significant data, their resolutions may not always be adequate for extensive field-scale studies [24, 77, 79]. Some researchers have emphasized the necessity of diverse and large training datasets to improve model generalization. They point out that models trained on small datasets may not perform well across locations and crop varieties [80, 81]. Lobell et al. (2020) found stronger generalization capabilities, potentially owing to the use of more thorough training datasets or better modelling algorithms, which our study might not have employed [82].

Future research should focus on improving ground-truth data quality and availability, enhancing model accuracy and generalization, optimizing algorithm efficiency, and improving integration with other data sources. Investing in data fusion techniques and automated ground-truthing methods can improve model accuracy and reliability. By addressing these recommendations, future research can build on current advancements, enhancing the accuracy, applicability, and accessibility of crop monitoring and yield estimation technologies, and contributing to more sustainable and efficient agricultural practices globally.

5. Conclusions

The VH time series indicated a significant difference in the growth patterns of rice varieties (2082, 27p31, 27p37, and Rajendra Bhagwati) grown in demo and control plots. Among all Sentinel-1 indices, the VH time series has been shown to be a useful tool for tracking crop calendars. Among the five yield models developed for estimating rice yields from Sentinel-1 and Sentinel-2-based indices, the GTB model performed better than the other models with an R^2 of 0.96 for the calibration dataset and 0.77 for the validation dataset. Based on this study, it can be concluded that the proposed methodology is useful for monitoring crops at the field scale to the district scale on a near-real-time basis. This approach uses open-source satellite data, which are finer in resolution, scalable, affordable, and less time-consuming; the GEE platform offers capabilities for storing data, performing analyses, and developing interactive maps. This study demonstrates the discrimination between different management practices using Sentinel-1-derived indices. Although our CMS demonstrated promising results for rice yield estimation, it is important to acknowledge that the study was based on a limited sample size (300/73 data points) and focused on a single crop within a specific region. These factors constrain the generalizability of the findings. Our findings are consistent with numerous studies on the limitations and potential of employing open-source satellite data and machine learning for crop monitoring and yield estimations. Although there is broad agreement on the problems of data quality, model generalization, computational complexity, and the necessity for good data integration, certain differences highlight areas where recent advances or alternative approaches have shown promise. Future research should expand on these advances by enhancing data quality and model robustness and addressing ethical concerns to improve the overall effectiveness and usefulness of these technologies in agriculture.

Abbreviations

AI	Artificial Intelligence
ALOS PALSAR	Advanced Land Observing Satellite Phased Array L-band Synthetic Aperture Radar
ANN	Artificial Neural Networks
ANOVA	Analysis of Variance
API	Applications Program Interface
CD	Critical Difference
CART	Classification and Regression Trees
CMS	Crop Monitoring System
DEM	Digital Elevation Model
DOS	Date of Sowing
DRF	Dr. Reddy Foundation
DT	Decision Trees
ESA	European Space Agency
GEE	Google Earth Engine
GRD	Ground Range Detected
GTB	Gradient Tree Boosting
LAI	Leaf Area Index
LSTM	Long Short-Term Memory
LULC	Land Use-Land Cover
ML	Machine Learning
MODIS	Moderate Resolution Imaging Spectroradiometer
MSI	Multispectral Instrument
NDVI	Normalized Differential Vegetation Index
NIR	Near-Infrared
RF	Random Forest
RMSE	Root Mean Squared Error
RS	Remote Sensing

SAR	Synthetic Aperture Radar
SPOT	Satellite Pour l'Observation de la Terre
SRTM	Shuttle Radar Topography Mission
SVR	Support Vector Regression
SVM	Support Vector Machines
SWIR	Short-wave Infrared
SWR	Stepwise Regression
VH	Vertical Horizontal Dual-polarized Band
VI	Vegetation Indices
VIF	Variance Inflation Factor
VV	Vertical-Vertical Dual-polarized Band

Acknowledgments

The authors want to acknowledge the grants, data, and cooperation received from the Dr. Reddy Foundation, India. We are also grateful to all the participating farmers and DRF field officers for their support in conducting field experiments and data collection.

Author Contributions

Srikanth Rupavatharam: Conceptualization, Funding acquisition, Investigation, Supervision, Writing – review & editing

Pranuthi Gogumalla: Conceptualization, Formal Analysis, Investigation, Methodology, Writing – original draft

Jameeruddin Shaik: Software, Visualization, Writing – original draft

Suman Saraswathibatla: Investigation, Project administration, Supervision

Mukund Patil: Validation, Writing – review & editing

Data Availability Statement

The data that support the findings of this study can be found at https://figshare.com/s/b611c04368825e6a028b (https://doi.org/10.6084/m9.figshare.29858924).

Conflicts of Interest

The authors declare no conflicts of interest.

References

[1] Mandapati, R., Gumma, M. K., Metuku, D. R., Bel-lam, P. K., Panjala, P., Maitra, S., Maila, N. Crop yield assessment using field-based data and crop models at the village level: A case study on a homogeneous rice area in Telangana, India. AgriEngineering. 2023, 5, 1909-1924. https://doi.org/10.3390/agriengineering5040117

[2] Nakalembe, C., Becker-Reshef, I., Bonifacio, R., Hu, G., Humber, M. L., Justice, C. J., Keniston, J., Mwangi, K., Rembold, F., Shukla, S. A review of satellite-based global agricultural monitoring systems available for Africa. Global Food Security. 2021, 29, 100543. https://doi.org/10.1016/j.gfs.2021.100543

[3] Radočaj, D., Obhođaš, J., Jurišić, M., Gašparović, M. Global open data remote sensing satellite missions for land monitoring and conservation: A review. Land. 2020, 9, 402. https://doi.org/10.3390/land9110402

[4] Restrepo, D. S., Pérez, L. E., López, D. M., Vargas-Cañas, R., Osorio-Valencia, J. S. Multi-dimensional dataset of open data and satellite images for characterization of food security and nutrition. Frontiers in Nutrition. 2022, 8, 796082. https://doi.org/10.3389/fnut.2021.796082

[5] Segarra, J., Buchaillot, M. L., Araus, J. L., Kefauver, S. C. Remote sensing for precision agriculture: Sentinel-2 improved features and applications. Agronomy. 2020, 10, 641. https://doi.org/10.3390/agronomy10050641

[6] Zhao, Y., Potgieter, A. B., Zhang, M., Wu, B., Hammer, G. L. Predicting wheat yield at the field scale by combining high-resolution Sentinel-2 satellite imagery and crop modelling. Remote Sensing. 2020, 12, 1024. https://doi.org/10.3390/rs12061024

[7] Niraimathi, J., Saravanan, S. Mapping and monitoring paddy crops with Sentinel-1 derived polarimetric parameters and machine learning. Environment, Development and Sustainability. 2025, 1-27. https://doi.org/10.1007/s10668-025-05313-3

[8] Singha, C., Swain, K. C. Rice crop growth monitoring with Sentinel-1 SAR data using machine learning models in Google Earth Engine cloud. Remote Sensing Applications: Society and Environment. 2023, 32, 101029. https://doi.org/10.1016/j.rsase.2023.101029

[9] Jiao, X., McNairn, H., Yekkehkhany, B., Dingle Robertson, L., Ihuoma, S. Integrating Sentinel-1 SAR and Sentinel-2 optical imagery with a crop structure dynamics model to track crop condition. International Journal of Remote Sensing. 2022, 43, 6509-6537. https://doi.org/10.1080/01431161.2022.2113055

[10] Amankulova, K., Farmonov, N., Omonov, K., Abdurakhimova, M., Mucsi, L. Integrating the Sentinel-1, Sentinel-2 and topographic data into soybean yield modelling using machine learning. Advances in Space Research. 2024, 73, 4052-4066. https://doi.org/10.1016/j.asr.2024.02.015

[11] Felegari, S., Sharifi, A., Moravej, K., Amin, M., Golchin, A., Muzirafuti, A., Tariq, A., Zhao, N. Integration of Sentinel-1 and Sentinel-2 satellite images for crop mapping. Applied Sciences. 2021, 11, 10104. https://doi.org/10.3390/app112110104

[12] Dadhwal, V., Ruhal, D., Medhavy, T., Jarwal, S., Khera, A., Singh, J., Sharma, T., Parihar, J. Wheat acreage estimation for Haryana using satellite digital data. Journal of the Indian Society of Remote Sensing. 1991, 19, 1-15. https://doi.org/10.1007/BF02904340

[13] Manjunath, K., Panigraphy, S., Chakraborty, M. Crop assessment using remote sensing—Part I: Crop acreage estimation. Indian Journal of Agricultural Economics. 2000, 55, 29-54.

[14] Potdar, M., Sharma, R., Dubey, R., Biswas, B. Relative performance of Landsat MSS, TM and IRS LISS-I data for acreage estimation of Rabi sorghum. Journal of the Indian Society of Remote Sensing. 1991, 19, 45-58. https://doi.org/10.1007/BF02904347

[15] Chakraborty, D., Saha, S., Saha, S. Use of space technology in agriculture: Innovations for a change of paradigm. In Innovations in Agriculture for a Self-Reliant India. CRC Press: Boca Raton, FL, USA; 2021, pp. 529-556.

[16] Wang, J., Wang, Y., Li, G., Qi, Z. Integration of remote sensing and machine learning for precision agriculture: A comprehensive perspective on applications. Agronomy. 2024, 14, 1975. https://doi.org/10.3390/agronomy14111975

[17] Surendran, U., Nagakumar, K. C. V., Samuel, M. P. Remote sensing in precision agriculture. In Digital Agriculture: A Solution for Sustainable Food and Nutritional Security. Springer: Singapore; 2024, pp. 201-223. https://doi.org/10.1007/978-981-99-6279-6_10

[18] Inoue, Y., Sakaiya, E., Wang, C. Potential of X-band images from high-resolution satellite SAR sensors to assess growth and yield in paddy rice. Remote Sensing. 2014, 6, 5995-6019. https://doi.org/10.3390/rs6075995

[19] Lopez-Sanchez, J. M., Cloude, S. R., Ballester-Berman, J. D. Rice phenology monitoring by means of SAR polarimetry at X-band. IEEE Transactions on Geoscience and Remote Sensing. 2011, 50, 2695-2709. https://doi.org/10.1109/TGRS.2011.2176740

[20] Koppe, W., Gnyp, M. L., Hütt, C., Yao, Y., Miao, Y., Chen, X., Bareth, G. Rice monitoring with multi-temporal and dual-polarimetric TerraSAR-X data. International Journal of Applied Earth Observation and Geoinformation. 2013, 21, 568-576. https://doi.org/10.1016/j.jag.2012.07.013

[21] Kobayashi, S., Ide, H. Rice crop monitoring using Sentinel-1 SAR data: A case study in Saku, Japan. Remote Sensing. 2022, 14, 3254. https://doi.org/10.3390/rs14143254

[22] Dineshkumar, C., Satishkumar, J. Rice crop monitoring using Sentinel-1 C-band data. International Archives of the Photogrammetry, Remote Sensing and Spatial Information Sciences. 2019, 42, 73-77. https://doi.org/10.5194/isprs-archives-XLII-3-W6-73-2019

[23] Hashemi, M. G., Abhishek, A., Jalilvand, E., Jayasinghe, S., Andreadis, K. M., Siqueira, P., Das, N. N. Assessing the impact of Sentinel-1 derived planting dates on rice crop yield modeling. International Journal of Applied Earth Observation and Geoinformation. 2022, 114, 103047. https://doi.org/10.1016/j.jag.2022.103047

[24] Veloso, A., Mermoz, S., Bouvet, A., Le Toan, T., Planells, M., Dejoux, J.-F., Ceschia, E. Understanding the temporal behavior of crops using Sentinel-1 and Sentinel-2-like data for agricultural applications. Remote Sensing of Environment. 2017, 199, 415-426. https://doi.org/10.1016/j.rse.2017.07.015

[25] Khabbazan, S., Vermunt, P., Steele-Dunne, S., Ratering Arntz, L., Marinetti, C., van der Valk, D., Iannini, L., Molijn, R., Westerdijk, K., van der Sande, C. Crop monitoring using Sentinel-1 data: A case study from The Netherlands. Remote Sensing. 2019, 11, 1887. https://doi.org/10.3390/rs11161887

[26] Yang, H., Pan, B., Li, N., Wang, W., Zhang, J., Zhang, X. A systematic method for spatio-temporal phenology estimation of paddy rice using time series Sentinel-1 images. Remote Sensing of Environment. 2021, 259, 112394. https://doi.org/10.1016/j.rse.2021.112394

[27] Manago, N., Hongo, C., Sofue, Y., Sigit, G., Utoyo, B. Transplanting date estimation using Sentinel-1 satellite data for paddy rice damage assessment in Indonesia. Agriculture. 2020, 10, 625. https://doi.org/10.3390/agriculture10120625

[28] Mandal, D., Kumar, V., Bhattacharya, A., Rao, Y. S., Siqueira, P., Bera, S. Sen4Rice: A processing chain for differentiating early and late transplanted rice using time-series Sentinel-1 SAR data with Google Earth Engine. IEEE Geoscience and Remote Sensing Letters. 2018, 15, 1947-1951. https://doi.org/10.1109/LGRS.2018.2864342

[29] Fikriyah, V. N., Darvishzadeh, R., Laborte, A., Khan, N. I., Nelson, A. Discriminating transplanted and direct seeded rice using Sentinel-1 intensity data. International Journal of Applied Earth Observation and Geoinformation. 2019, 76, 143-153. https://doi.org/10.1016/j.jag.2018.11.007

[30] Wangkheimayum, N., Paliwal, H. Development of rice yield forecasting model using linear regression for Imphal West District, Manipur, India. International Journal of Environment and Climate Change. 2023, 13, 485-490. https://doi.org/10.9734/ijecc/2023/v13i121650

[31] Sellam, V., Poovammal, E. Prediction of crop yield using regression analysis. Indian Journal of Science and Technology. 2016, 9, 1-5. https://doi.org/10.17485/ijst/2016/v9i38/91714

[32] Gumma, M. K., Kadiyala, M., Panjala, P., Ray, S. S., Akuraju, V. R., Dubey, S., Smith, A. P., Das, R., Whitbread, A. M. Assimilation of remote sensing data into crop growth model for yield estimation: A case study from India. Journal of the Indian Society of Remote Sensing. 2022, 50, 257-270. https://doi.org/10.1007/s12524-021-01393-8

[33] Huang, Y., Hakim, B., Zammataro, S. Measuring the carbon footprint of road construction using CHANGER. International Journal of Pavement Engineering. 2013, 14, 590-600. https://doi.org/10.1080/10298436.2012.721552

[34] Palanivel, K., Surianarayanan, C. An approach for prediction of crop yield using machine learning and big data techniques. International Journal of Computer Engineering and Technology. 2019, 10, 110-118. https://doi.org/10.34218/IJCET.10.2.2019.017

[35] Van Klompenburg, T., Kassahun, A., Catal, C. Crop yield prediction using machine learning: A systematic literature review. Computers and Electronics in Agriculture. 2020, 177, 105709. https://doi.org/10.1016/j.compag.2020.105709

[36] Dang, C., Liu, Y., Yue, H., Qian, J., Zhu, R. Autumn crop yield prediction using data-driven approaches: Support vector machines, random forest, and deep neural network methods. Canadian Journal of Remote Sensing. 2021, 47, 162-181. https://doi.org/10.1080/07038992.2021.1884933

[37] Mariano, C., Monica, B. A random forest-based algorithm for data-intensive spatial interpolation in crop yield mapping. Computers and Electronics in Agriculture. 2021, 184, 106094. https://doi.org/10.1016/j.compag.2021.106094

[38] Jeong, S., Ko, J., Yeom, J.-M. Predicting rice yield at pixel scale through synthetic use of crop and deep learning models with satellite data in South and North Korea. Science of the Total Environment. 2022, 802, 149726. https://doi.org/10.1016/j.scitotenv.2021.149726

[39] Attema, E., Cafforio, C., Gottwald, M., Guccione, P., Guarnieri, A. M., Rocca, F., Snoeij, P. Flexible dynamic block adaptive quantization for Sentinel-1 SAR missions. IEEE Geoscience and Remote Sensing Letters. 2010, 7, 766-770. https://doi.org/10.1109/LGRS.2010.2046233

[40] Drusch, M., Del Bello, U., Carlier, S., Colin, O., Fernandez, V., Gascon, F., Hoersch, B., Isola, C., Laberinti, P., Martimort, P. Sentinel-2: ESA's optical high-resolution mission for GMES operational services. Remote Sensing of Environment. 2012, 120, 25-36. https://doi.org/10.1016/j.rse.2011.11.026

[41] Gorelick, N., Hancher, M., Dixon, M., Ilyushchenko, S., Thau, D., Moore, R. Google Earth Engine: Planetary-scale geospatial analysis for everyone. Remote Sensing of Environment. 2017, 202, 18-27. https://doi.org/10.1016/j.rse.2017.06.031

[42] Gao, B.-C. NDWI—A normalized difference water index for remote sensing of vegetation liquid water from space. Remote Sensing of Environment. 1996, 58, 257-266. https://doi.org/10.1016/S0034-4257(96)00067-3

[43] Louis, J., Debaecker, V., Pflug, B., Main-Knorn, M., Bieniarz, J., Mueller-Wilm, U., Cadau, E., Gascon, F. Sentinel-2 Sen2Cor: L2A processor for users. In Living Planet Symposium 2016, ESA SP-740. 2016, pp. 9-13.

[44] Tucker, C. J., Elgin Jr, J., McMurtrey III, J., Fan, C. Monitoring corn and soybean crop development with hand-held radiometer spectral data. Remote Sensing of Environment. 1979, 8, 237-248. https://doi.org/10.1016/0034-4257(79)90010-6

[45] Gamon, J. A., Serrano, L., Surfus, J. The photochemical reflectance index: An optical indicator of photosynthetic radiation use efficiency across species, functional types, and nutrient levels. Oecologia. 1997, 112, 492-501. https://doi.org/10.1007/s004420050337

[46] Gitelson, A. A., Merzlyak, M. N., Lichtenthaler, H. K. Detection of red edge position and chlorophyll content by reflectance measurements near 700 nm. Journal of Plant Physiology. 1996, 148, 501-508. https://doi.org/10.1016/S0176-1617(96)80285-9

[47] Wang, L., Qu, J. J. NMDI: A normalized multi-band drought index for monitoring soil and vegetation moisture with satellite remote sensing. Geophysical Research Letters. 2007, 34, L20405. https://doi.org/10.1029/2007GL031021

[48] Galvao, L. S., Formaggio, A. R., Tisot, D. A. Discrimination of sugarcane varieties in southeastern Brazil with EO-1 Hyperion data. Remote Sensing of Environment. 2005, 94, 523-534. https://doi.org/10.1016/j.rse.2004.11.010

[49] Dhanya, V., Subeesh, A., Kushwaha, N., Vishwakarma, D. K., Kumar, T. N., Ritika, G., Singh, A. Deep learning based computer vision approaches for smart agricultural applications. Artificial Intelligence in Agriculture. 2022, 6, 211-229. https://doi.org/10.1016/j.aiia.2022.09.004

[50] Subeesh, A., Mehta, C. Automation and digitization of agriculture using artificial intelligence and internet of things. Artificial Intelligence in Agriculture. 2021, 5, 278-291. https://doi.org/10.1016/j.aiia.2021.07.001

[51] Araújo, S. O., Peres, R. S., Barata, J., Lidon, F., Ramalho, J. C. Characterising the Agriculture 4.0 landscape—Emerging trends, challenges and opportunities. Agronomy. 2021, 11, 667. https://doi.org/10.3390/agronomy11040667

[52] Kapse, M., Sharma, V., Poulose, J., Elangovan, N., Mahajan, Y. Cotton Health-Guard: AI-enhanced crop health assessment through image classification. In Industrial Applications of Big Data, AI, and Blockchain. IGI Global: Hershey, PA, USA; 2024, pp. 204-219. https://doi.org/10.4018/978-1-6684-7080-6.ch013

[53] Singh, R. K., Kumar, P., Kumar, M., Tyagi, K., Jain, H. Artificial machine learning-based classification of land cover and crop types using Sentinel-2A imagery. Sustainable Agriculture Systems and Technology. 2022, 326-336. https://doi.org/10.1007/978-981-19-4956-2_27

[54] Zheng, H., Chen, L., Han, X., Zhao, X., Ma, Y. Classification and regression tree (CART) for analysis of soybean yield variability among fields in Northeast China: The importance of phosphorus application rates under drought conditions. Agriculture, Ecosystems & Environment. 2009, 132, 98-105. https://doi.org/10.1016/j.agee.2009.03.004

[55] Choudhary, K., Shi, W., Dong, Y., Paringer, R. Random forest for rice yield mapping and prediction using Sentinel-2 data with Google Earth Engine. Advances in Space Research. 2022, 70, 2443-2457. https://doi.org/10.1016/j.asr.2022.06.004

[56] Arumugam, P., Chemura, A., Schauberger, B., Gornott, C. Remote sensing based yield estimation of rice (Oryza sativa L.) using gradient boosted regression in India. Remote Sensing. 2021, 13, 2379. https://doi.org/10.3390/rs13122379

[57] Zununjan, Z., Turghan, M. A., Sattar, M., Kasim, N., Emin, B., Abliz, A. Combining the fractional order derivative and machine learning for leaf water content estimation of spring wheat using hyper-spectral indices. Plant Methods. 2024, 20, 97. https://doi.org/10.1186/s13007-024-01234-3

[58] Howell, J. F., Games, P. A. The robustness of the analysis of variance and the Tukey WSD test under various patterns of heterogeneous variances. Journal of Experimental Education. 1973, 41, 33-37. https://doi.org/10.1080/00220973.1973.11011321

[59] Seifert, E. OriginPro 9.1: Scientific data analysis and graphing software—Software review. Journal of Statistical Software. 2014. https://doi.org/10.18637/jss.v059.b01

[60] Mishra, V. Examining the growth and instability of major crops across agro-climatic zones in Bihar. Lloyd's Business Review. 2025, 170-193.

[61] Zanaga, D., Van De Kerchove, R., Daems, D., De Keersmaecker, W., Brockmann, C., Kirches, G., Wevers, J., Cartus, O., Santoro, M., Fritz, S. ESA WorldCover 10 m 2021 V200. European Space Agency: Paris, France; 2022. https://doi.org/10.5281/zenodo.5571936

[62] Zhang, Y., Sui, B., Shen, H., Wang, Z. Estimating temporal changes in soil pH in the black soil region of Northeast China using remote sensing. Computers and Electronics in Agriculture. 2018, 154, 204-212. https://doi.org/10.1016/j.compag.2018.09.020

[63] Balz, T., Soergel, U., Crespi, M., Osmanoglu, B. Advances in SAR: Sensors, methodologies, and applications. MDPI: Basel, Switzerland; 2018. ISBN 3-03897-182-0.

[64] Harfenmeister, K., Spengler, D., Weltzien, C. Analyzing temporal and spatial characteristics of crop parameters using Sentinel-1 backscatter data. Remote Sensing. 2019, 11, 1569. https://doi.org/10.3390/rs11131569

[65] Clauss, K., Ottinger, M., Leinenkugel, P., Kuenzer, C. Estimating rice production in the Mekong Delta, Vietnam, utilizing time series of Sentinel-1 SAR data. International Journal of Applied Earth Observation and Geoinformation. 2018, 73, 574-585. https://doi.org/10.1016/j.jag.2018.07.021

[66] de Bem, P. P., de Carvalho Júnior, O. A., de Carvalho, O. L. F., Gomes, R. A. T., Guimarães, R. F., Pimentel, C. M. M. Irrigated rice crop identification in southern Brazil using convolutional neural networks and Sentinel-1 time series. Remote Sensing Applications: Society and Environment. 2021, 24, 100627. https://doi.org/10.1016/j.rsase.2021.100627

[67] Cao, J., Zhang, Z., Tao, F., Zhang, L., Luo, Y., Zhang, J., Han, J., Xie, J. Integrating multi-source data for rice yield prediction across China using machine learning and deep learning approaches. Agricultural and Forest Meteorology. 2021, 297, 108275. https://doi.org/10.1016/j.agrformet.2020.108275

[68] Pham, H. T., Awange, J., Kuhn, M., Nguyen, B. V., Bui, L. K. Enhancing crop yield prediction utilizing machine learning on satellite-based vegetation health indices. Sensors. 2022, 22, 719. https://doi.org/10.3390/s22030719

[69] Son, N.-T., Chen, C.-F., Cheng, Y.-S., Toscano, P., Chen, C.-R., Chen, S.-L., Tseng, K.-H., Syu, C.-H., Guo, H.-Y., Zhang, Y.-T. Field-scale rice yield prediction from Sentinel-2 monthly image composites using machine learning algorithms. Ecological Informatics. 2022, 69, 101618. https://doi.org/10.1016/j.ecoinf.2022.101618

[70] Ahmad, M. W., Mourshed, M., Rezgui, Y. Trees vs neurons: Comparison between random forest and ANN for high-resolution prediction of building energy consumption. Energy and Buildings. 2017, 147, 77-89. https://doi.org/10.1016/j.enbuild.2017.04.038

[71] Gopal, P. M., Bhargavi, R. A novel approach for efficient crop yield prediction. Computers and Electronics in Agriculture. 2019, 165, 104968. https://doi.org/10.1016/j.compag.2019.104968

[72] Mekonnen, Y., Namuduri, S., Burton, L., Sarwat, A., Bhansali, S. Machine learning techniques in wireless sensor network based precision agriculture. Journal of the Electrochemical Society. 2019, 167, 037522. https://doi.org/10.1149/1945-7111/ab6038

[73] Hoang-Phi, P., Nguyen-Kim, T., Nguyen-Van-Anh, V., Lam-Dao, N., Le-Van, T., Pham-Duy, T. Rice yield estimation in An Giang Province, the Vietnamese Mekong Delta using Sentinel-1 radar remote sensing data. IOP Conference Series: Earth and Environmental Science. 2021, 652, 012001. https://doi.org/10.1088/1755-1315/652/1/012001

[74] Najafi, P., Eftekhari, A., Sharifi, A. Evaluation of time-series Sentinel-2 images for early estimation of rice yields in south-west of Iran. Aircraft Engineering and Aerospace Technology. 2023, 95, 741-748. https://doi.org/10.1108/AEAT-04-2022-0100

[75] Soriano-González, J., Angelats, E., Martínez-Eixarch, M., Alcaraz, C. Monitoring rice crop and yield estimation with Sentinel-2 data. Field Crops Research. 2022, 281, 108507. https://doi.org/10.1016/j.fcr.2022.108507

[76] Wu, B., Zhang, M., Zeng, H., Tian, F., Potgieter, A. B., Qin, X., Yan, N., Chang, S., Zhao, Y., Dong, Q. Challenges and opportunities in remote sensing-based crop monitoring: A review. National Science Review. 2023, 10, nwac290. https://doi.org/10.1093/nsr/nwac290

[77] Khanal, S., Kc, K., Fulton, J. P., Shearer, S., Ozkan, E. Remote sensing in agriculture—Accomplishments, limitations, and opportunities. Remote Sensing. 2020, 12, 3783. https://doi.org/10.3390/rs12223783

[78] Yang, L., Driscol, J., Sarigai, S., Wu, Q., Chen, H., Lippitt, C. D. Google Earth Engine and artificial intelligence (AI): A comprehensive review. Remote Sensing. 2022, 14, 3253. https://doi.org/10.3390/rs14143253

[79] Houborg, R., McCabe, M. F. High-resolution NDVI from Planet's constellation of Earth observing nano-satellites: A new data source for precision agriculture. Remote Sensing. 2016, 8, 768. https://doi.org/10.3390/rs8090768

[80] You, J., Li, X., Low, M., Lobell, D., Ermon, S. Deep Gaussian process for crop yield prediction based on remote sensing data. In Proceedings of the 31st International Conference on Machine Learning. 2017, Vol. 31. https://doi.org/10.48550/arXiv.1705.09535

[81] Kussul, N., Lavreniuk, M., Skakun, S., Shelestov, A. Deep learning classification of land cover and crop types using remote sensing data. IEEE Geoscience and Remote Sensing Letters. 2017, 14, 778-782. https://doi.org/10.1109/LGRS.2017.2681128

[82] Lobell, D. B., Azzari, G., Burke, M., Gourlay, S., Jin, Z., Kilic, T., Murray, S. Eyes in the sky, boots on the ground: Assessing satellite- and ground-based approaches to crop yield measurement and analysis. American Journal of Agricultural Economics. 2020, 102, 202-219. https://doi.org/10.1093/ajae/aaz051

Biography

Srikanth Rupavatharam is Head of the Innovations Hub (iHub) and Senior Scientist in Digital Agriculture at ICRISAT, India. He earned his PhD in Postharvest Technologies from Massey University, New Zealand, and a Master's in the same field from Writtle College, University of Essex, UK. He is a Marshall Papworth Scholar and received the Gardner's Prize (2005) for excellence in horticulture, as well as the Helen E. Akers PhD scholarship awarded via the Global Challenges Research Fund's David Livingstone Fellowship, University of Strathclyde. With over 23 years of experience, he has led agricultural R&D projects across the UK, Africa, New Zealand, and India; his work focuses on non-destructive quality assessment, AI and Big Data for decision support, UAVs, and digital tools to aid smallholder farmers. He has published more than 25 research articles to date.

Pranuthi Gogumalla is a Scientist in Digital Agriculture at ICRISAT, Patancheru, India. She earned her PhD in Irrigation Water Management from IIT Roorkee, a Master's in Satellite Meteorology and Weather Informatics from Jawaharlal Nehru Technological University, Hyderabad, and a Bachelor's in Agricultural Sciences from Acharya N. G. Ranga Agricultural University. Her research focuses on remote sensing, GIS, and climate-smart agricultural applications including evapotranspiration modelling, soil and water conservation, agro-meteorology, and weather-based advisories. She has authored over twenty research papers and contributed to tools such as the Meghdoot mobile app for location-specific agro-advisories in India.

Jameeruddin Shaik is a Scientific Officer at the International Crops Research Institute for the Semi-Arid Tropics (ICRISAT), Patancheru (Hyderabad, India). He works primarily in remote sensing and Geographic Information Systems (GIS) for agricultural applications. His skills include RS/GIS mapping, sustainable agriculture, climate change related to agriculture, and using tools such as ESRI GIS and Google EarthEngine.

Suman Saras leads Rural Livelihoods, Climate Action & Environment programs at Dr. Reddy's Foundation. He holds over 20 years of experience designing and implementing development models for underserved rural communities. He has been instrumental in scaling up Dr. Reddy's Foundation's initiatives such as MITRA, which has impacted tens of thousands of marginal farmers by promoting sustainable farming practices, input service enhancement, digital tools, and climate-resilient solutions. Suman's work emphasizes scalable, low-cost interventions, regenerative agriculture models, women's empowerment in rural economies, and ecosystem restoration. He regularly represents DRF in national and regional forums on climate action, agriculture, and livelihoods.

Mukund Patil is a Senior Scientist in Soil Physics at the International Crops Research Institute for the Semi-Arid Tropics (ICRISAT), India. He earned his Ph.D. in Soil Physics from IIT Kharagpur with research focused on vadose-zone hydrology in rice fields. His expertise spans soil physics, watershed management, and digital agriculture, and he has led and contributed to several watershed programs across Karnataka, Telangana, Odisha, and Maharashtra aimed at improving farmer livelihoods through sustainable resource management. He also works on developing digital platforms and smart agricultural tools in collaboration with national and international partners, with a strong focus on climate-smart practices such as crop residue management, direct-seeded rice (DSR), alternate wetting and drying, and optimized nutrient use to reduce emissions. He has additionally served on the methodologies expert panel for India's Carbon Credit Trading Scheme, highlighting his contributions to soil science, digital agriculture, and climate resilience.

Research Field

Srikanth Rupavatharam: Post Harvest Technology, Remote sensing and digital agriculture, Generative Artificial Intelligence for agricultural innovations, AI-enabled pest and disease diagnostics, Carbon farming and Green-house gas mitigation.

Pranuthi Gogumalla: Digital Monitoring, Reporting and Verification for carbon farming, Remote sensing in agriculture, Climate change impacts on crop systems, Agrometeorology, Crop modeling and simulation studies.

Jameeruddin Shaik: Satellite and Drone Remote Sensing, Mobile and Web Application Development, Image data Analysis, Generative AI, Database Management.

Suman Saras: Rural livelihoods and skill development, Sustainable agriculture and food security, Climate-resilient farming practices, Youth employability and vocational training, Education access and digital learning.

Mukund Patil: Soil Physics, Digital agriculture and data analytics, Agricultural knowledge management systems, Land Resource Inventory systems, Digital Monitoring, Reporting and Verification.